



Contents lists available at ScienceDirect

**Mechanical Systems and Signal Processing**journal homepage: [www.elsevier.com/locate/ymssp](http://www.elsevier.com/locate/ymssp)**Fault detection in rotor bearing systems using time frequency techniques****N. Harish Chandra, A.S. Sekhar\****Department of Mechanical Engineering, Indian Institute of Technology Madras, Chennai 600036, India***ARTICLE INFO****Article history:**

Received 28 November 2014

Received in revised form

28 October 2015

Accepted 13 November 2015

**Keywords:**

Rotor bearing system

Fault Diagnosis

Wavelet transform

Hilbert Huang Transform

**ABSTRACT**

Faults such as misalignment, rotor cracks and rotor to stator rub can exist collectively in rotor bearing systems. It is an important task for rotor dynamic personnel to monitor and detect faults in rotating machinery. In this paper, the rotor startup vibrations are utilized to solve the fault identification problem using time frequency techniques. Numerical simulations are performed through finite element analysis of the rotor bearing system with individual and collective combinations of faults as mentioned above. Three signal processing tools namely Short Time Fourier Transform (STFT), Continuous Wavelet Transform (CWT) and Hilbert Huang Transform (HHT) are compared to evaluate their detection performance. The effect of addition of Signal to Noise ratio (SNR) on three time frequency techniques is presented. The comparative study is focused towards detecting the least possible level of the fault induced and the computational time consumed. The computation time consumed by HHT is very less when compared to CWT based diagnosis. However, for noisy data CWT is more preferred over HHT. To identify fault characteristics using wavelets a procedure to adjust resolution of the mother wavelet is presented in detail. Experiments are conducted to obtain the run-up data of a rotor bearing setup for diagnosis of shaft misalignment and rotor stator rubbing faults.

© 2015 Elsevier Ltd. All rights reserved.

**1. Introduction**

To identify existing faults in rotor bearing systems, several researchers have proposed theories and methods based on Fourier spectrum analysis, Orbit analysis, Wavelet Transforms and Hilbert Huang Transform [1,2]. In general common faults like the unbalance, shaft cracks, coupling misalignment and rotor-stator rub are identified based on the vibration data acquired. To identify these faults many researchers have focused on steady state vibration data [3] and few have presented their observations based on run-up and run-down vibration data [1,2,4,5]. Prabhakar et al. [6] have considered two individual cases of misalignment and shaft crack and presented their findings. The present study focuses on using run-up vibration responses for identifying coupling misalignment, shaft crack and rotor-stator rub faults. These three faults are expected to develop during the operation. Also, during operation secondary faults like rotor-stator rub [7] or impact can be caused due to the presence of primary faults like misalignment and unbalance. Many fault classification approaches based on neural networks and support vector machines are also based on steady-state vibration data. These require baseline or the healthy machine's data to reveal the fault information.

\* Corresponding author.

E-mail addresses: [97mechari@gmail.com](mailto:97mechari@gmail.com) (N.H. Chandra), [as\\_sekhar@iitm.ac.in](mailto:as_sekhar@iitm.ac.in) (A.S. Sekhar).

Many researchers have presented model based methods for identification of faults such as fatigue crack [8] and coupling misalignment [9]. For large rotating machinery Pennacchi et al. [10,11] have presented a model based method for fault identification. A least square identification technique is introduced to identify faults in frequency domain. Model based approaches are useful not only for fault diagnosis but also have been applied to other technical processes [12]. A review on model based fault detection and quantification methods is reported by Lees et al. [13]. In a rotor bearing system misalignment may extent to premature failure of other components like bearing, seals and couplings. Rotating machinery with excessive misalignment causes high vibration and lowers the life of the components.

Alignment estimation methods based on optical laser or dial indicators are applicable only when the rotor system is stationary and the misalignment correction based on these instruments is based on the stationary data of the machine. Also, most of the industrial rotating machinery may not be available directly for examination due to limitations on deconstruction or size. Thus, to obtain a promising alignment, diagnosis based on vibration based data is unavoidable. Steady state or run-up vibration responses can be utilized to detect the misalignment present in the system [3,6]. Usually, steady state vibration based method leads to a confounding spectral information [14] and consumes more time when compared to run-up response based diagnosis. Based on steady state vibration data, the spectral information obtained for a particular fault configuration can be confusing as per the available literature [3]. The vibration with high  $2\times$  and  $4\times$  harmonics are commonly agreed for the presence of misalignment fault [15]. However, defects like fatigue crack and stiffening effects on shafts (due to rubbing), also show high  $2\times$  harmonic vibrations. Sekhar and Prabhu [16] used higher order FEM to study the effect of misalignment. Using the theory based on kinematic model of the couplings Xu and Marangoni [17] reported a detection method based on the higher harmonics developed in the response due to misalignment. Under similar alignment conditions it is possible that for different types of couplings different spectral information can exist [14]. The spectral information of the steady state vibration response clearly cannot distinguish the existence faults.

For rotor supported on fluid film bearing, faults such as oil whirl, oil whip or dry whip can exist. Using run-up vibration data of such rotors Fan et al. [18] reported the diagnosis procedure for rotor supported on journal bearings. Since theoretical methods for fault detection include many assumptions results based on such methods may not be directly applicable for signals obtained from actual systems. Thus, experimental study is always necessary for examining new methods. Identification of multiple faults in rotor bearing systems is presented by Bachschmid et al. [19]. They have reported a least squares identification technique in frequency domain for crack diagnosis.

Many vibration based fault diagnosis tools such as full Fourier transform [3], Wavelet transform [20], empirical mode decomposition (EMD) [21], Hilbert Huang Transform (HHT) [1] and algorithms based on support vector machines (SVM) or Classifiers [22] are available. It is necessary to understand every tool, to choose an appropriate diagnosis method for the fault detection.

In rotating machinery fatigue cracks can develop due to varying loads and continuous operation. In order to develop techniques to detect existing cracks in rotor-bearing systems based on the vibration response of machinery, crack shafts have to be modeled accurately and its response needs to be studied thoroughly. Cracks in structures such as beams or shafts are modeled in many ways. The presence of crack causes local flexibility i.e., decreases its stiffness, reduces its natural frequency and also affects its vibration behavior. The added flexibility due to the presence of crack can be expressed in the form of a matrix which is very suitable for FEM modeling of cracked rotors. This matrix was developed by Papadopoulos and Dimarogonas [23]. The stiffness of the cracked element varies with respect to the shaft rotation continuously, due to breathing behavior of the crack. This behavior is modeled by expressing stiffness variation by a truncated cosine series, which results in higher harmonics of running frequency in the FFT of vibration response.

The probability of rotor-stator rubbing is also high due to the presence of small clearances. Beatty [24] reported that to evaluate a rotor to stator rub contact phenomenon, monitoring steady state vibration response is not sufficient. Since, a transient signal like start-up response covers possible range of amplitudes it contains more information when compared to steady state vibration data. Also, monitoring through run-up vibration data consumed less time and facilitates early detection of the rub fault. Torkhani et al. [25] presented an experimental investigation to detect light, medium and heavy partial rub impacts using transient excitation. Muszynska [26] reported a detailed literature review on rotor to stator contact problems. Recently, Patel and Darpe [2] solved the rub initiation diagnosis problem using Hilbert-Huang Transform and compared the results with wavelet transforms.

The objective of this study is to detect multiple faults existing in a rotor system, using run-up vibrations. In this study both simulations and experimental investigations of misalignment, shaft crack and rotor-stator rub fault detection are considered. Use of HHT algorithm is highlighted along with a comparative study using the STFT and CWT approaches. The effect of signal to noise ratio for detecting faults using the three time frequency techniques is investigated.

The fault parameters considered for simulation study and experimental study are different. The objective of the simulation study is to identify least possible fault diagnosis features. For example for the simulation study, 0.075 mm rub clearance is considered as the heavy rub case, on the other hand for experiments 0.1 mm rub clearance case is considered as heavy rub. The reason being that for experiments, for rub clearance below 0.1 mm, the response obtained was very unstable and the rotor could not reach or cross the critical speed. In case of experiments, the vibration data corresponding to the least measurable fault parameter is considered for study. The vibration data recorded is considered for testing only if repeatability of harmonic signature is observed. In Section 2, the finite element model of the rotor bearing system is presented, which includes the theoretical modeling of faults. A brief overview of the time frequency techniques adopted in this study is

presented in [Section 3](#). In [Section 4](#), the simulation results considering individual and collective combination of faults are presented. In [Section 5](#), experimental results are presented followed by conclusions in [Section 6](#).

## 2. Finite element modeling of rotor system with faults

The idea of modeling faults is to understand the dynamics of the rotor system where influences of the fault parameters like location and magnitude can be studied easily. It is also possible to study the interaction between different faults, especially when they simultaneously exist in the system. These faults are theoretically modeled as equivalent forces that are expected to be acting on a healthy system. These forces and moments show the same effects on the system as the faults effect the real system. These loads depend on the parameters which are based on the faults. Through a detailed study on dynamic behavior due to faults, different inferences specific to individual fault can be drawn and can be used to detect faults in damaged systems. These theoretical models can also be used to detect the location and magnitude of faults in the system when correlated with measured vibrations of damaged system. However, accuracy of identified fault is dependent on the theoretical fault model which is used to model the actual fault. In the literature, fault models for the unbalance, coupling misalignment, shaft crack, rotor bow, and rotor rub, etc. are available. In the present work, unbalance, misalignment, rotor stator rub and crack are detected using different identification techniques. Thus, the theoretical models of these faults are discussed briefly in the following subsections.

### 2.1. Equation of motion

A rotor supported on rolling element bearings with a rigid disk placed at the center of the rotor is considered for simulations. Euler-Bernoulli beam elements are used to model the shaft elements and the coupling elements. A finite element model for rotor bearing systems reported by Nelson and McVaugh [27] is used in simulations.

Rotational degrees of freedom ( $\theta$  along horizontal and  $\phi$  along vertical direction) and translational degrees of freedom ( $x$  along horizontal and  $y$  along vertical direction) are assumed. The finite element model is formulated by assembling the elemental mass, stiffness, gyroscopic and damping matrices of the rotor system [27]. The nodal displacement and force vectors are also considered as per the boundary conditions. The computational work for finite element analysis is performed using MATLAB R2012a software. The schematic diagram of the rotor system model considered for simulations and experiments in this paper is as shown in [Fig. 1](#).

#### 2.1.1. Rotor disk

Disk is considered to be rigid and is modeled using mass and mass moment of inertia terms at the corresponding nodes. For a rotor running with constant spin speed, the equation of motion [27] for the rigid disk is given by

$$([M_T^d] + [M_R^d])\{\ddot{u}^d\} - \omega[G^d]\{\dot{u}\} = \{U^d\} \quad (1)$$

where  $M_T^d$  is the translational mass matrix of the disk,  $M_R^d$  is the rotational mass matrix of disk,  $u = \{x \ y \ \theta \ \phi\}'$ , and  $[G^d]$  is the gyroscopic matrix of the disk element. The term  $U^d$  of Eq. (1) represents the forcing term on the disk. Forces include unbalance and interconnecting forces, etc.

#### 2.1.2. Rolling element bearings

Generally, roller bearings are employed for high speed applications. The equation of motion for the bearing components is given by

$$[C^b]\{\dot{u}^b\} + [K^b]\{u^b\} = \{U^b\} \quad (2)$$

where  $u^b = [x \ y]'$ ,  $K^b = \begin{bmatrix} k_{xx}^b & 0 \\ 0 & k_{yy}^b \end{bmatrix}$ ,  $C^b = \begin{bmatrix} c_{xx}^b & 0 \\ 0 & c_{yy}^b \end{bmatrix}$ ,  $U^b$  represent the forcing vector of the bearings,  $[K^b]$  and  $[C^b]$  are the stiffness and damping matrices of the bearings respectively. The bearing stiffnesses are assumed as isotropic and without cross coupled stiffness terms.

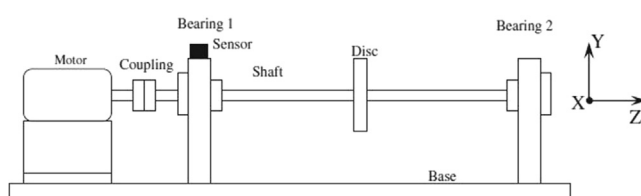


**Fig. 1.** Schematic of rotor bearing system.

### 2.1.3. Shaft element

The equation of motion of the shaft element can be written as shown below:

$$([M_T^e] + [M_R^e])\{\ddot{u}^e\} - \omega[G^e]\{\dot{u}\} + [K_B^e]\{u^e\} = \{U^e\} \quad (3)$$

where  $M_T^e$  is the translational mass matrix and,  $M_R^e$  is the rotational mass matrix of shaft element,  $[K_B^e]$  is the bending stiffness matrix of the shaft element and  $[G_e]$  is the gyroscopic matrix. The forcing function  $U^e$  of Eq. (3) includes unbalance forces, interconnected forces and other external loads on the shaft. Internal energy of the shafts is not considered in the present study.

### 2.1.4. Unbalance in rigid disk

Unbalance is a primary source of vibration in rotating machinery. Some level of residual unbalance always exists due to manufacturing defects and assembly. For the steady state vibration case the unbalance forces along  $x$  and  $y$  directions are as shown below:

$$F_x = me\omega^2 \cos(\omega t) \quad (4)$$

$$F_y = me\omega^2 \sin(\omega t) \quad (5)$$

The unbalance forces for a rotor with angular acceleration ( $\alpha$ ) and angular rotation  $\psi$  are as shown below:

$$F_x = me(\ddot{\psi} \sin(1/2\alpha t^2) + \psi^2 \cos(1/2\alpha t^2)) \quad (6)$$

$$F_y = me(-\ddot{\psi} \cos(1/2\alpha t^2) + \psi^2 \sin(1/2\alpha t^2)) \quad (7)$$

These unbalance forces are placed on the nodes corresponding to the disk element as shown in Fig. 2. The angular rotation  $\psi$  of the shaft due to acceleration is obtained by using the following relationship  $\psi(t) = \omega_0 t + 1/2(\alpha t^2)$ .

### 2.1.5. Assembled equations of motion

For the rotor bearing system the assembled equation of motion is obtained as shown below:

$$[M]\{\ddot{u}\} + [C]\{\dot{u}\} + [K]\{u\} = \{U\} \quad (8)$$

where  $[M]$ ,  $[C]$  and  $[K]$  correspond to the mass, damping and stiffness of the components respectively. The damping matrix  $[C]$  includes the damping from the bearings and the gyroscopic terms.

The finite element model of the rotor system is presented in Fig. 2.  $U$  is the excitation matrix which contains unbalance, rotor-stator rub and misalignment fault induced external forces.

## 2.2. Misalignment modeling

Misalignment in rotor bearing systems leads to development of reaction loads at the coupling location. The misalignment can be parallel, angular or combination of both parallel and angular cases. These reaction forces corresponding to different types of misalignment are modeled by Sekhar and Prabhu [16]. These loads are acting as periodic loads on the rotating shafts with a periodic function of half-sinusoidal having time period of  $\pi/\Omega$  [28]. In the present analysis,  $1 \times \Omega$ ,  $2 \times \Omega$ ,  $3 \times \Omega$  and  $4 \times \Omega$  components of the reaction forces are considered for finite element simulations. To represent the reaction loads at coupling location a coordinate system model for both types of misalignment is presented by Sekhar and Prabhu [16] as shown in Fig. 3. The reaction loads for two shafts with axes  $Z_1$  and  $Z_2$  are given below.

For parallel misalignment case:

$$\begin{aligned} MX1 &= T_q \sin \theta_1 + K_b \phi_1, & MX2 &= T_q \sin \theta_2 + K_b \phi_2 \\ MY1 &= T_q \sin \phi_1 + K_b \theta_1, & MY2 &= T_q \sin \phi_2 + K_b \theta_2 \\ FX1 &= (-MY1 - MY2)/Z3, & FX2 &= -FX1 \\ FY1 &= (MX1 + MX2)/Z3, & FY2 &= FY1 \end{aligned} \quad (9)$$

For angular misalignment case:

$$MX1 = 0, \quad MX2 = -K_b \theta, \quad MY1 = 0$$

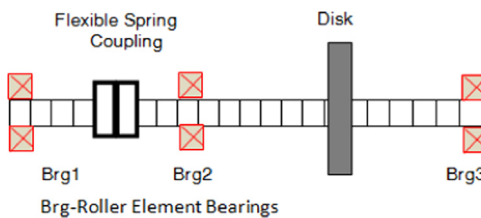


Fig. 2. Finite element model of the rotor bearing system.

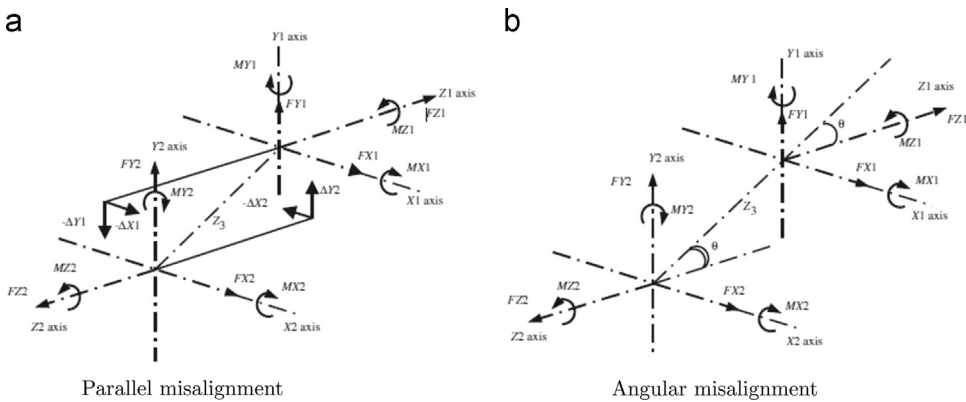


Fig. 3. Coupling coordinate system [16].

$$\begin{aligned} MY2 &= T_q \sin \theta, \quad MZ1 = T_q / \cos \theta, \quad MZ2 = -T_q \\ FX1 &= (-MY1 - MY2)/Z3, \quad FX2 = -FX1 \\ FY1 &= (MX1 + MX2)/Z3, \quad FY2 = -FY2 \end{aligned} \quad (10)$$

where in Eqs. (9) and (10),  $F1$  and  $F2$  are the reaction forces,  $M1$  and  $M2$  are the reaction moments corresponding to  $Z_1$  and  $Z_2$  shaft axes,  $T_q$  is the torque,  $\Delta_{ij}$  is the misalignment introduced (for  $i=X$  and  $Y$  directions and  $j=1, 2$ ),  $Z_3$  is the center of articulation,  $\theta$  and  $\phi$  are the misalignment angles,  $\theta_1 = \sin^{-1}(\Delta X_1/Z_3)$ ,  $\theta_2 = \sin^{-1}(\Delta X_2/Z_3)$ ,  $\phi_1 = \sin^{-1}(\Delta Y_1/Z_3)$ ,  $\phi_2 = \sin^{-1}(\Delta Y_2/Z_3)$  and  $K_b$  is the bending spring rate per degree per disk pack of the coupling.

In the present study, since run-up vibrations are considered for fault diagnosis, along with unbalance forces, without doubt the misalignment forces are also functions of angular acceleration ( $\alpha$  rad/s<sup>2</sup>). The angular displacement  $\theta = \omega t$  in terms of angular acceleration can be expressed as  $\theta = \omega t = (1/2)\alpha t^2$ . Corresponding to  $1 \times \omega t$  harmonic the reaction force harmonic component is  $0.5\alpha t^2$ , for  $2 \times \omega t$  harmonic is  $\alpha t^2$ , for  $3 \times \omega t$  harmonic is  $1.5\alpha t^2$  and finally for  $4 \times \omega t$  harmonic is  $2\alpha t^2$ . Thus, the force vectors ( $\{Q_c^1\}$  and  $\{Q_c^2\}$ ) as shown in Eqs. (11) and (12) correspond to the left and right nodes of the coupling element:

$$\{Q_c^1\} = \left\{ \begin{array}{l} FX1 \sin 0.5\alpha t^2 + FX1 \sin \alpha t^2 + FX1 \sin 1.5\alpha t^2 + FX1 \sin 2\alpha t^2 \\ FY1 \cos 0.5\alpha t^2 + FY1 \cos \alpha t^2 + FY1 \cos 1.5\alpha t^2 + FY1 \cos 2\alpha t^2 \\ 0 \\ 0 \end{array} \right\} \quad (11)$$

$$\{Q_c^2\} = \left\{ \begin{array}{l} FX2 \sin 0.5\alpha t^2 + FX2 \sin \alpha t^2 + FX2 \sin 1.5\alpha t^2 + FX2 \sin 2\alpha t^2 \\ FY2 \cos 0.5\alpha t^2 + FY2 \cos \alpha t^2 + FY2 \cos 1.5\alpha t^2 + FY2 \cos 2\alpha t^2 \\ 0 \\ 0 \end{array} \right\} \quad (12)$$

### 2.3. Shaft crack modeling

Mathematical modeling of a transverse breathing crack is presented in this section. The local flexibility due to the existence of a crack in structural member can be modeled by a flexibility matrix. The order of this matrix depends upon the degrees of freedom of the finite element model. The elements of the flexibility matrix for a shaft with a crack were computed by Papadopoulos and Dimarogonas [29]. In the present analysis,  $4 \times 4$  matrix having the elements corresponding to the two lateral and two angular degrees of freedom about horizontal and vertical directions are considered. Due to the presence of a crack only the stress field near to the crack gets affected. This implies that the elemental stiffness matrix remains unchanged, but for the cracked element as shown in Fig. 4(a) the stiffness variation is significant. Shaft with a cracked element is presented as shown in Fig. 4(b).

The element present on the right hand side of a cracked element can be considered an external force and on the other hand the left hand side elements can be considered as constraints. With this assumption the elements of the flexibility matrix of a cracked element can be realized. The flexibility matrices which are function of dimensionless crack depth ( $c/D$ ) for a fully open crack and half open and half-closed cases as presented by Sekhar and Prabhu [30] are considered in the present study.

Total flexibility of a cracked section is obtained by adding local flexibility of cracked section to the flexibility of the uncracked section given by

$$[C] = [C_0] + [C_c] \quad (13)$$

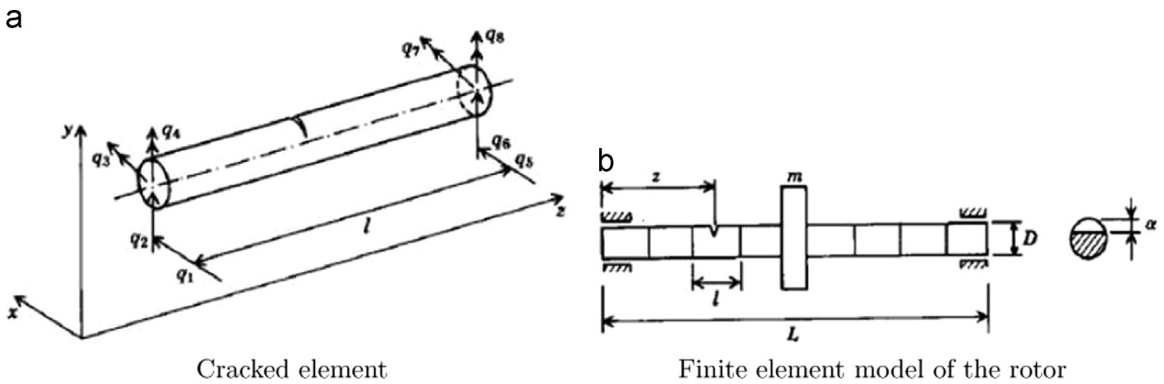


**Fig. 4.** (a) Cracked element and (b) finite element model of the rotor.

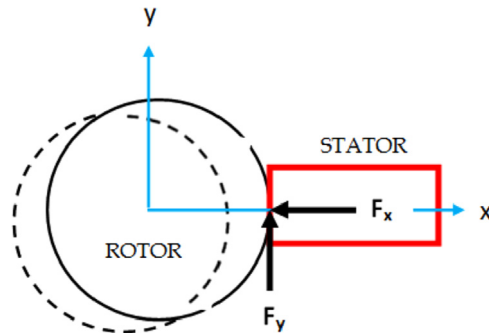


**Fig. 5.** Rub impact of the rotor.

where  $[C_0]$  is the flexibility matrix of an uncracked element and  $[C_c]$  is the flexibility matrix corresponding to the additional strain energy due to the presence of crack. The stiffness matrix of the shaft element with crack can be obtained by

$$[K_c] = [T][C]^{-1}[T]^T \quad (14)$$

where  $[T]$  is the transformation matrix [30]. During operation due to the presence of the crack the stiffness of the cracked element varies with respect to time or the angular orientation. Thus the variation in stiffness can be expressed as a function with truncated cosine terms as shown below:

$$[K_{cb}] = [K_0] + [K_1] \cos \omega t + [K_2] \cos 2\omega t + [K_3] \cos 3\omega t + [K_4] \cos 4\omega t \quad (15)$$

where  $[K_1], [K_2], [K_3]$  and  $[K_4]$  are fitting coefficient matrices [30].

#### 2.4. Rotor-stator rub impact modeling

Rubbing phenomenon can exist in many forms and many rotating components based on the orientation of the stator and rotors are subjected to annular or radial rubbing. In any of the above two cases, nonlinear rubbing forces in horizontal and vertical directions of rotor are generated. It is obvious due to the high amplitude of rotor vibrations the rub impact occurs if a stator or a limiter exists. The rub-impact plane is shown in Fig. 5, where the tangential force  $F_t = -F_y$  and radial force  $F_N = -F_x$ .

A frictional relationship based on coulomb theory is used to model the contact forces. The nonlinear impact loads generated during rub-impact event are given as [31],

$$F_x = -k_s(x - \delta)h \quad (16)$$

$$F_y = -fk_s(x - \delta)h \quad (17)$$

where  $\delta$  is the initial clearance,  $x$  is the response of the rotor,  $f$  is the frictional coefficient and the function  $h$  is equal to 1 if  $x < \delta$  and else it is 0. Rotor rubbing impact occurs occasionally and last for very short span of time. The stiffness ( $k_s$ ) of the stator is high compared to the rotor and the impact is considered as an elastic phenomenon.

### 3. Overview of time frequency techniques

In the following sub-sections, the time frequency techniques used in the present study for fault diagnosis are discussed briefly. Using time-frequency techniques, a review on rotor fault diagnosis is reported by Feng et al. [32] and Yan et al. [20].

#### 3.1. Short Time Fourier Transform (STFT)

STFT is also called windowed Fourier transform, it is used to examine the features of a response with respect to time. For a vibration response  $y(t)$ , with  $w(\tau-t)$  as the window function centered at time  $t$ , the response  $y(t)$  using this window function is  $y(t)w(\tau-t)$ . Shifting the function  $w(\tau-t)$  along the time axis of the response and employing the Fourier analysis to every window components lead to the following integral [32]:

$$\text{STFT}_y(t, f) = \int_{-\infty}^{\infty} y(\tau)g(\tau-t)e^{-2\pi f\tau} d\tau \quad (18)$$

#### 3.2. Continuous Wavelet Transform (CWT)

Continuous Wavelet Transform uses basis functions with translation and dilation parameters instead of simple complex exponentials unlike Fourier transform [32]. It adds a dilation parameter along with a time translation parameter to the analysis. Hence, it is best suited for time-frequency analysis, and is effective in analyzing non-stationary signals like run-up vibration data of the rotor. CWT of a time signal  $y(t)$  is obtained by solving the following convolution integral:

$$\text{CWT}_y(t, a) = \frac{1}{\sqrt{a}} \int_{-\infty}^{\infty} y(\tau)\psi\left(\frac{t-\tau}{a}\right) d\tau \quad (19)$$

In the present work Complex Morlet (CMOR) wavelet function is chosen as the base wavelet.

#### 3.3. Hilbert–Huang Transform (HHT)

The HHT algorithm is an adaptive non-parametric tool. Time frequency tools such as STFT and CWT are based on linearity assumption and thus involve a convolution integral. The HHT does not involve in convolution integral thus basis function is not necessary to obtain the time-frequency representation of the signal. The HHT is a unique method which is suitable for non-linear and non-stationary responses [1] of the system. To obtain Hilbert Huang Transform a response firstly one has to estimate the (1) empirical mode decomposition (EMD) to obtain the Intrinsic Mode Functions (IMFs) and (2) the IMFs should be processed with Hilbert Transform to obtain the instantaneous frequency corresponding to each IMF [33].

Although, EMD approach presents remarkable performance in analyzing non-stationary vibration data, the algorithm has few disadvantages. Issues related to the empirical mode decomposition like lack of theoretical proof, edge effects, threshold for stopping the sifting [34] exist if the Intrinsic Mode Functions are not well defined. The dot product computed among different IMFs should be evaluated to estimate the loss of energy (orthogonality). For the EMD procedure to be accurate, the vibration data should be verified for the intrinsic mode functions being orthogonal with respect to other IMFs. The disadvantages of EMD can be solved by using the Ensembled EMD approach which is an improvement over the former version of EMD algorithm.

## 4. Simulation results

In this section, simulation results for fault detection in a rotor bearing system are presented. Firstly, transient signals obtained from individual faults are considered and later the combined effects of these faults are studied on the finite element model discussed in Section 2. To obtain the flexural run-up vibration data of the rotor bearing system, the equations of motion as presented in Eq. (8) are numerically solved using Houbolt-Time marching technique. The excitation matrix  $U$  which includes loads generated due to different faults is also assembled in the global equations of motion. For the nodes corresponding to the disk, the run-up unbalance forces as presented in Eq. (6) and (7) are applied. The specifications of the rotor bearing system considered for the simulations are the same as the experimental setup discussed in Section 5 and given in Table 4. Houbolt Time marching technique with an integration time step of 0.001 s is used to solve the global equations of motion in MATLAB 2012 software. For different angular acceleration levels the rotor is excited above its first critical speed ( $\omega_{n1} = 48.6$  Hz).

Fig. 6 presents the case of a healthy rotor run-up response with an angular acceleration of 20 rad/s<sup>2</sup>, the rotor crosses the first critical speed in 18.5 s. For this case only unbalance forces are considered, since unbalance is an inevitable fault. This data (Fig. 6) serves as a base line information which is used to compare the rotor response with faults. However, using the time-frequency techniques presented in this paper, the existence of the faults can be identified even when the base line data is unavailable. Detection of misalignment, crack and rub is presented in Sections 4.1, 4.2 and 4.3 respectively. In Section 4.4, rotor response with combined faults is obtained and conclusions are made to distinguish individual faults.

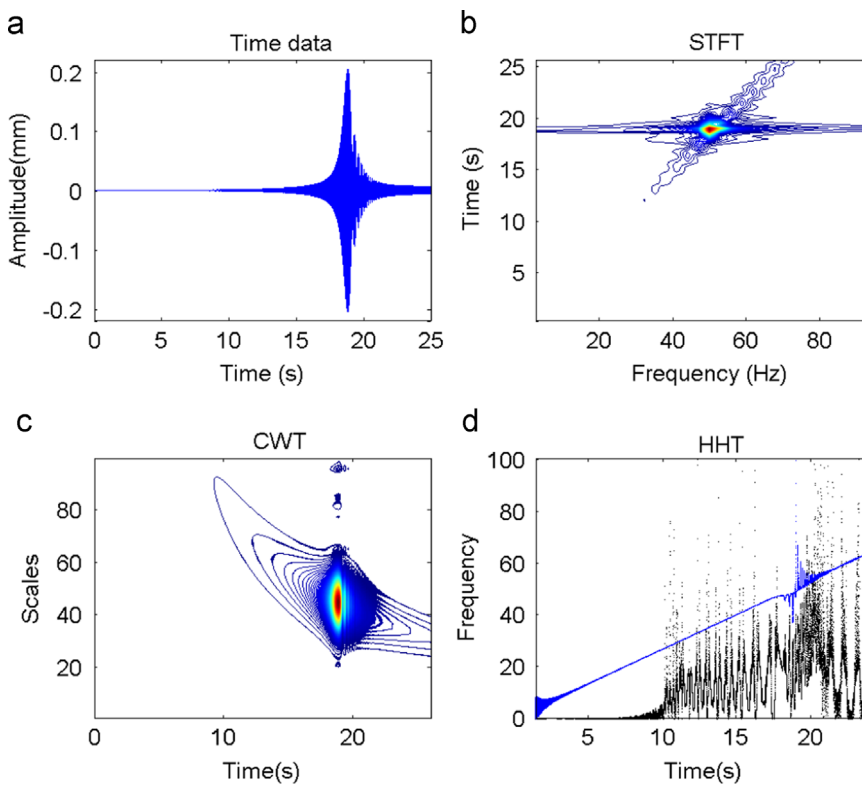


**Fig. 6.** Healthy rotor run-up response (without faults)  $\alpha = 20 \text{ rad/s}^2$  and (a) run-up time data, (b) STFT, (c) Complex Morlet wavelet CWT and (d) the Hilbert Huang Transform plot-blue: IMF1 and Black: IMF2. (For interpretation of the references to color in this figure caption, the reader is referred to the web version of this paper.)

#### 4.1. Misalignment detection using time frequency techniques

To identify the misalignment fault using time frequency techniques the finite element model of the rotor bearing system including a flexible coupling is considered for simulations. The reaction forces generated in the rotor coupling bearing system due to misalignment are obtained using the coupling coordinate system as presented in Section 2. These misalignment forces (Eqs. (11) and (12)) generated at the coupling location are introduced into the nodal excitation vector  $U$ . For different types and levels of misalignment the run-up vibration data is acquired to study the misalignment effects. Three cases of parallel misalignment (high, medium and low levels with  $\Delta x = 1.5 \text{ mm}$ ,  $0.8 \text{ mm}$ , and  $0.01 \text{ mm}$  are considered respectively) and angular misalignment case (with  $\theta=2^\circ$ ) are considered for numerical investigation. Figs. 7–12 present the misalignment fault diagnosis results for different cases. For a healthy system without faults the diagnosis results are presented in Fig. 6. For high and medium parallel misalignment cases the diagnosis results are presented in Figs. 7 and 8 respectively. For these two cases all the three time-frequency techniques considered were successful in identifying the misalignment fault features.

As presented in Fig. 7(a), the subharmonics due to misalignment can be noticed in time domain data also. But, for medium (Fig. 8) and low (Fig. 10) cases of misalignment the subharmonics are hardly visible in the time data. As observed from Fig. 7(b and c) both STFT and CWT tools are capable of detecting the misalignment fault as the subharmonics are clearly noticed. Whereas, STFT in case of Fig. 8 detects the fault barely, while from Fig. 10 fault is undetected. As presented in Section 3, HHT algorithm involves in (a) EMD and (b) Hilbert transform of the IMFs obtained in the previous step.

Unlike other signal processing techniques, the HHT involves in EMD process which is decomposition in the time domain and will not elucidate the signal data by simplifications on the stationary and linear characteristics of the response [1]. By not considering these simplifications a sharper resolution in both time and frequency domain representations is noted using the HHT algorithm.

Among 12 IMFs obtained using EMD, the first four components of run-up vibration data for different cases of misalignment estimated using by Empirical Mode Decomposition algorithm are presented in Fig. 9. The orthogonality of the IMFs is checked by estimating the dot product among IMFs. After confirming the independence of these functions, the Hilbert Huang spectrum is obtained from the IMF data. The dot product estimated among the IMFs was found close to zero. In addition to the dot product, the energy of the intrinsic mode functions and the final residue were also obtained. The cumulative sum of energy levels of each IMF and the final residue is estimated as 191.6, which is close to the energy of the

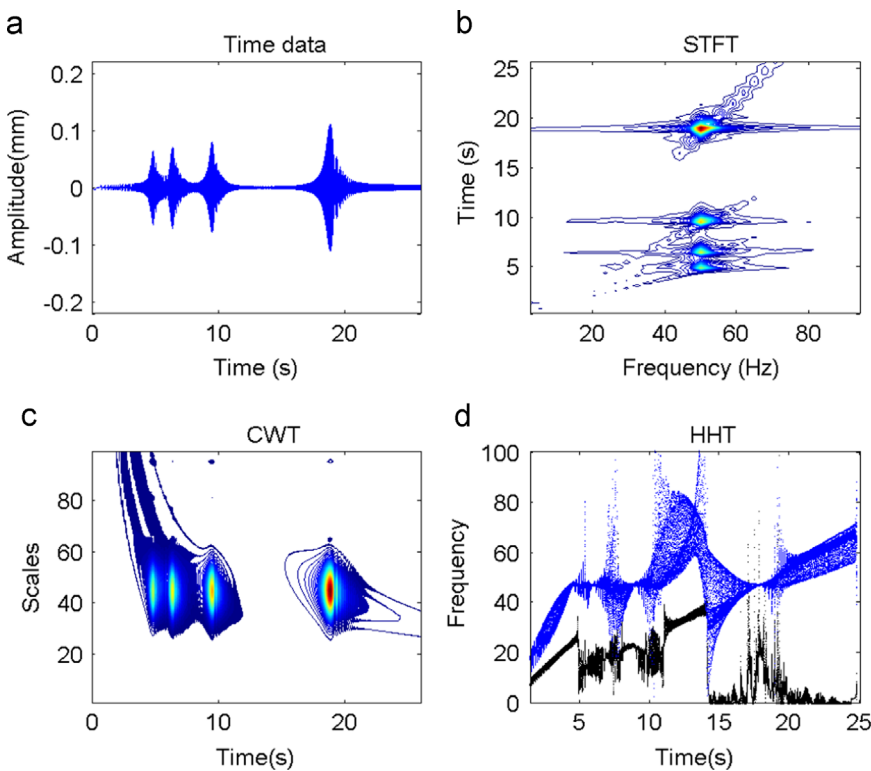


**Fig. 7.** Diagnosis results for high parallel misalignment case  $\Delta x = 1.5$  mm with angular acceleration  $\alpha = 20 \text{ rad/s}^2$ , (a) run-up time data, (b) STFT spectrogram, (c) Complex Morlet wavelet CWT scalogram and (d) the HHT plot-blue: IMF1 and black: IMF2. (For interpretation of the references to color in this figure caption, the reader is referred to the web version of this paper.)

run-up vibration data (189.8) acquired from the finite element model. Thus it is confirmed that EMD procedure for the run-up vibration data for the rotor bearing system considered in this study is conservative w.r.t. energy.

For low misalignment case, fault features are not clearly distinguishable from the IMF1 data. However, analysis by employing the Hilbert Huang Transform transform as presented below could detect the fault features very clearly even for the lower case of misalignment.

The performance of HHT technique in revealing a sharper resolution in time and frequency domains can be appreciated through the analysis presented in Fig. 10(d). For no misalignment run-up data (Fig. 6(d)), since the instantaneous frequency is increasing steadily without any interruptions a straight line is observed as expected. This is due to the fact that HHT algorithm is not based on time and frequency uncertainty principle, it formulated based on the instantaneous frequency estimate. Because of the characteristics, the Hilbert Huang Transform is successful in identifying slightest changes in frequencies with high resolution which are unidentified in time domain data as well as STFT spectrograms. These frequency variations are observed due to the existence of subharmonics generated due to the misalignment.

The computation time required for CWT depends on many parameters. The computation time required by the CWT tool for different parameters are presented in Table 1. The computation time consumed by HHT algorithm considering the full length run-up response is 45 s, whereas the time consumed by CWT is 321 s. However, as shown in Fig. 10(c) CWT could not identify the fault clearly. For such situations, Wavelet Zooming has to be employed to detect the fault clearly. Even though, the sub-critical harmonics go unnoticed in the CWT result as seen from Fig. 10(c), it is possible to identify the fault features by choosing the resolution parameters correctly. Since the subharmonics are expected to be present at fractional multiples of critical speed, the time interval between 4 and 12 s of the run-up response is focused. Now, considering the signal only in this time region and processing it with wavelets reveal the fault characteristics as shown in Fig. 11(a), but with a poor resolution along time axis. This resolution can be improved by choosing right band frequency for the mother wavelet. The mother wavelet used in this study is the Complex Morlet (CMOR) Wavelet transform. Basically, CMOR has two parameters to adjust the resolution. The band frequency parameter ( $F_b$ ) improves the time resolution and the center frequency parameter ( $F_c$ ) controls the frequency resolution. A large value of  $F_b$  generates a wavelet which is shorter in time and reveals the information accurately. On the other hand increasing the value of  $F_c$  demands more scale inputs which indirectly demands more computation time. The computation time increases if the values of  $F_b$  and  $F_c$  are high. In Fig. 10(c) the values of  $F_c$  and  $F_b$  considered are 1 Hz and 1.5 Hz respectively. Now by adjusting  $F_b$  and  $F_c$  both to 1.5 Hz, the harmonics due to misalignment are clearly seen in Fig. 11(d). For angular misalignment case among all the time-frequency techniques the Hilbert Huang Transform is a better choice since it has shown appreciable performance (Fig. 12) in terms of resolution and

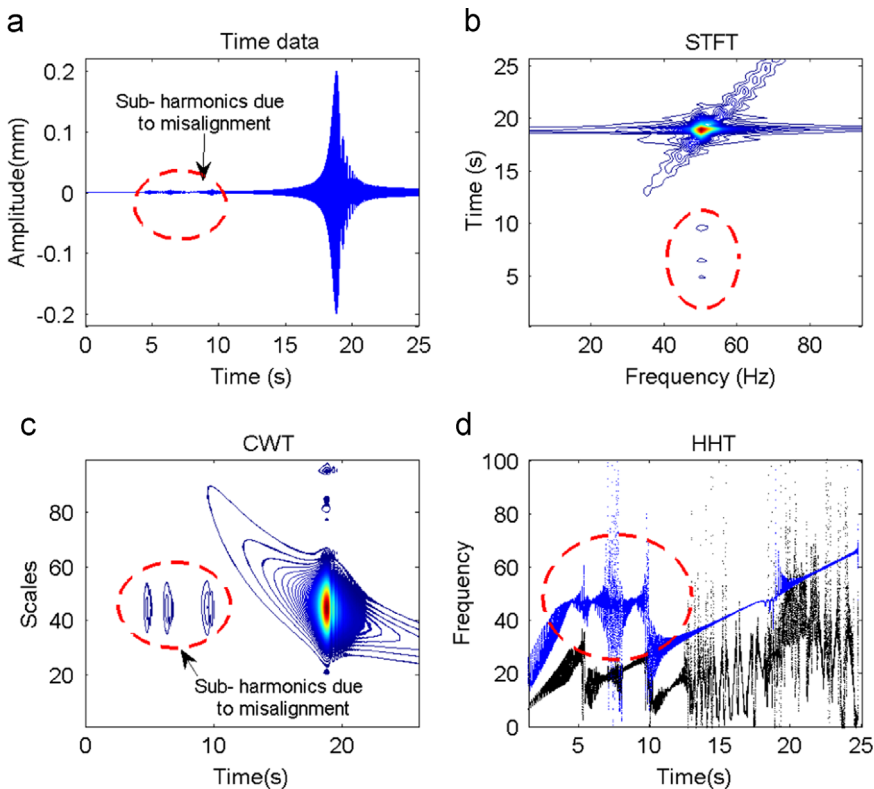


**Fig. 8.** Diagnosis results for medium parallel misalignment  $\Delta x = 0.8$  mm with angular acceleration  $\alpha = 20$  rad/s<sup>2</sup>, (a) run-up time data, (b) STFT spectrogram, (c) Complex Morlet wavelet CWT scalogram and (d) the HHT plot-blue: IMF1 and black: IMF2. (For interpretation of the references to color in this figure caption, the reader is referred to the web version of this paper.)

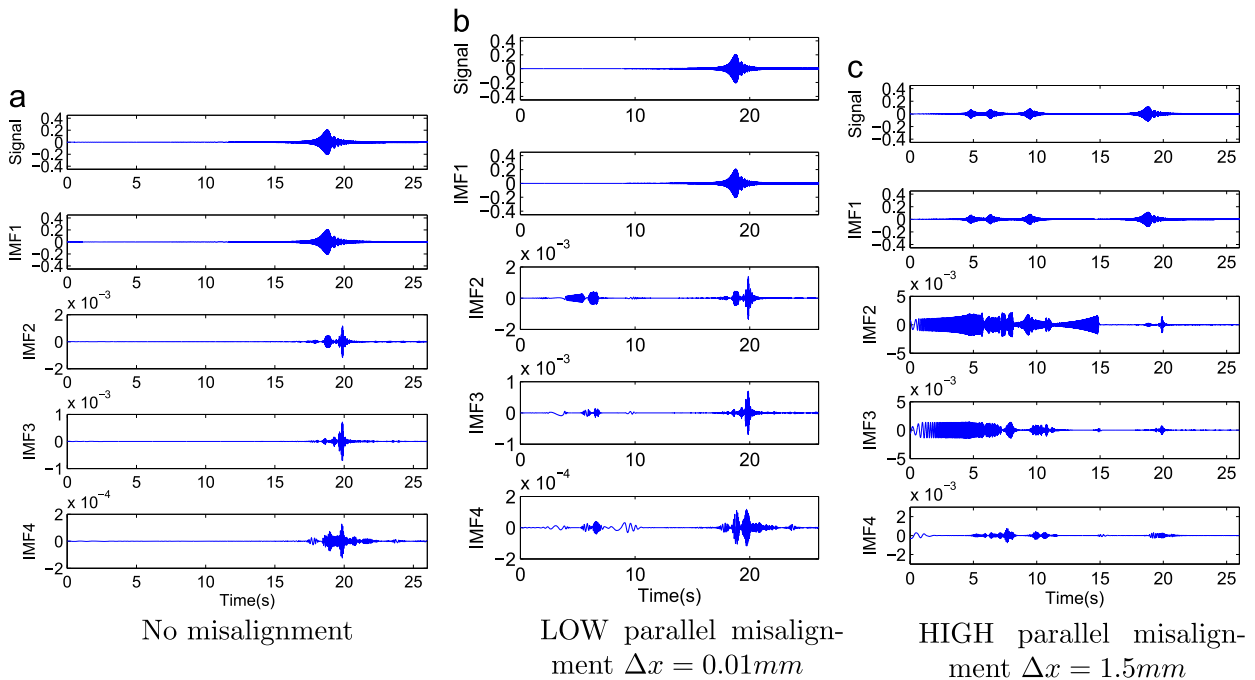


**Fig. 9.** Empirical mode decomposition for different misalignment cases.

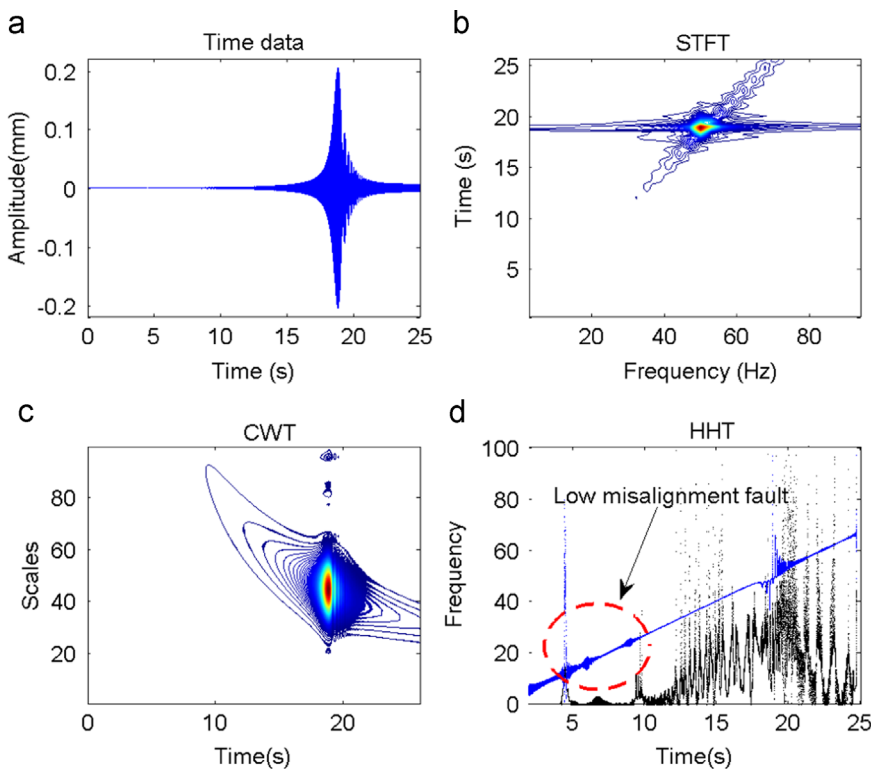


**Fig. 10.** Fault diagnosis results for low parallel misalignment  $\Delta x = 0.01$  mm with  $\alpha = 20$  rad/s<sup>2</sup>, (a) run-up time data, (b) STFT, (c) CWT scalogram and (d) the HHT plot-blue: IMF1 and black: IMF2. (For interpretation of the references to color in this figure caption, the reader is referred to the web version of this paper.)

consumes less computation time. Variation in the forces caused due to misalignment leads to smooth fluctuations in the signals at the corresponding harmonics and both CWT and HHT were able to diagnose the fault. In the above CWT analysis, Complex Morlet wavelet transform is employed, using other wavelets which will also serve the purpose for fault detection. As explained higher values of  $F_b$  and  $F_c$  consume more computation time. When compared to HHT based diagnosis, CWT technique thus consumes more computation time.

#### 4.2. Crack detection using time–frequency techniques

The finite element modeling of a rotor bearing system with a transverse breathing crack is presented in Section 2.3. The fault diagnosis results for a rotor without crack (without any fault) are presented earlier in Fig. 6. For different crack depths the run-up signals are acquired and are processed using time frequency techniques. The response and signal analysis for large and small cracks are presented in Figs. 13 and 14 respectively. Periodic asymmetry in the stiffness of the cracked rotors leaves a harmonic signature as presented in these figures. Similar observations have been reported in [1,35]. However in the present study methods to improve the performance of CWT and HHT to detect even smaller cracks and to overcome low SNR are presented.

As shown in Fig. 14, the existence of the small crack goes unnoticed in time and STFT data. Improving the resolution of CWT by adjusting the  $F_b$  and  $F_c$  values to 1.5 Hz as presented in the previous section, the presence of the subharmonic due to crack is detected. A strong sub-critical harmonic component at  $0.5 \times$  the critical speed and very weak higher sub-critical components present in the run-up response represents the presence of crack in a shaft. As observed in the misalignment detection, even for crack detection the time consumed by HHT algorithm is less when compared to the CWT based diagnosis method.

#### 4.3. Rotor–stator rub detection using time–frequency analysis

Two cases of rubbing phenomenon are considered in this study. First case is a heavy rubbing against a limiter, where the clearance value  $\delta_1 = 0.075$  mm and a light rub case with  $\delta_1 = 0.155$  mm are simulated. The run-up response is best suited signal to detect rub fault, the penetration of the rotors response into the stator is represented in Fig. 15.

The orbit response of the rotor without rub fault is presented in Fig. 16. The diagnosis results for heavy rub and light rub-impact cases are presented in Figs. 17 and 18 respectively. It is identified that the rub impact against a limiter only affects the

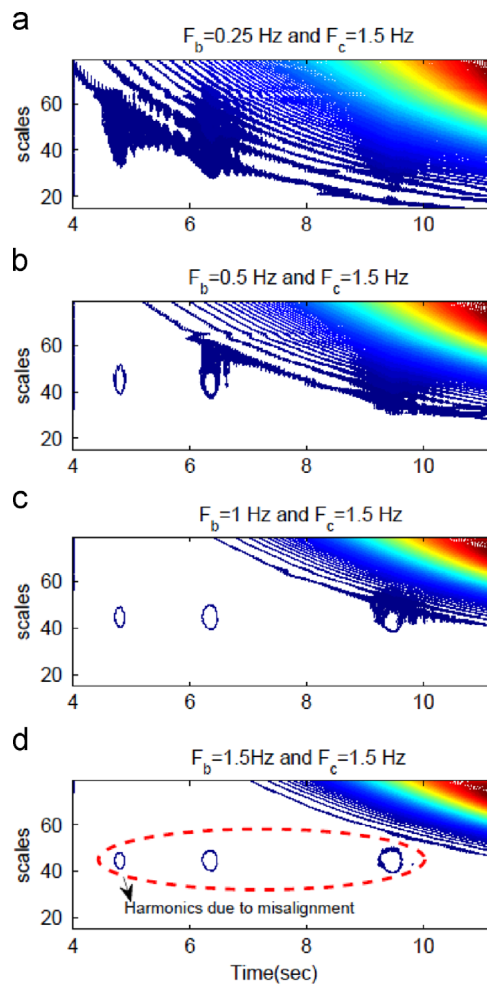


**Fig. 11.** Wavelet scalogram with different resolution.

healthy rotor response near critical speed. A split in the critical speed as also observed by Bedoor [4] is evident from Fig. 17. By comparing the results presented in Figs. 17 and 18 with healthy rotors response as shown in Fig. 6, it can be concluded that a run-up response with rub-impact against a limiter shows its effects when the response is higher at the critical speed. In case of light rub impact as shown in Fig. 18, the time and STFT data could not reveal the split near the resonance, whereas CWT and HHT clearly identify the rub-impact against the stator. Also, for this case no clear backward whirl or split near the resonance is observed in the time and the orbit response data. However, when significantly heavy rub-impact forces exist the orbit response of the rotor is presented in Fig. 19. The initiation of backward whirl due to heavy rub is clearly evident in this figure, by comparing with healthy rotors case as shown in Fig. 16, the split at the resonance is evident.

#### 4.4. Comparison of fault characteristics

Considering a case in which all the above three faults exist (see Fig. 20) reveals few interesting conclusions. As shown in Fig. 20(d), the effect of misalignment causes rapid increase in the instantaneous frequency of the signal at different harmonics. However, the influence of crack and rub-impact were significant only at  $1/2 \times$  and  $1 \times$  critical harmonics respectively.

From the results presented in previous sections it is observed that  $0.5 \times$  and the other harmonic components strongly coexist if misalignment is present in the system. Whereas in case of rotor with crack the critical components other than  $0.5 \times$  are weak in magnitude. However, if both misalignment and crack coexist the subharmonic components add up. As presented in Fig. 20(c), a common harmonic component exists for crack and misalignment at  $0.5 \times$  critical component. However, a rub impact affects the response at the critical speed. The presence of the rub-impact can be identified from the split observed at the resonance. As presented in Section 4.2 a smaller crack depth will not produce sub-critical harmonics other than  $0.5 \times$ . However, if these harmonics exist an alternative approach has to be adopted. To differentiate the crack and

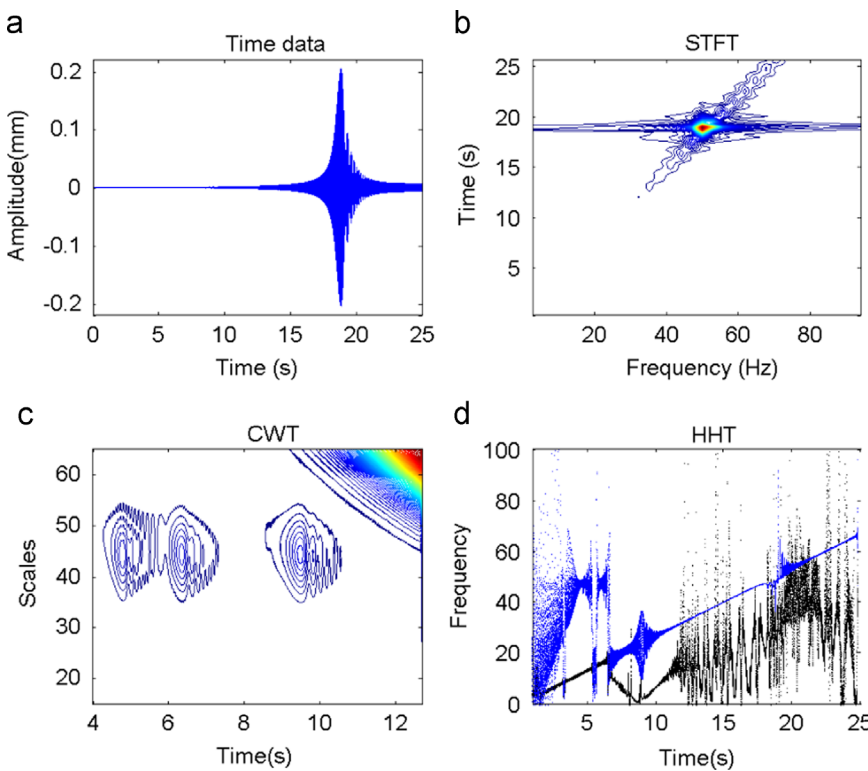


**Fig. 12.** Angular misalignment  $\theta = 2^\circ$  and  $\alpha = 20 \text{ rad/s}^2$ , (a) run-up vibration data, (b) STFT, (c) Complex Morlet wavelet scalogram and (d) the HHT plot-blue: IMF1 and black: IMF2. (For interpretation of the references to color in this figure caption, the reader is referred to the web version of this paper.)

**Table 1**

Computation time consumed by CWT for different resolution.

Length of the signal	Wavelet resolution	Scales in steps of 2	CWT computation time (s)
Full signal (0–25 s)	$F_b = 1 \text{ Hz}, F_c = 1.5 \text{ Hz}$	1–100	321
4–12 s	$F_b = 0.25 \text{ Hz}, F_c = 1.5 \text{ Hz}$	15–65	86
4–12 s	$F_b = 0.5 \text{ Hz}, F_c = 1.5 \text{ Hz}$	15–65	96.7
4–12 s	$F_b = 1 \text{ Hz}, F_c = 1.5 \text{ Hz}$	15–65	110.5
4–12 s	$F_b = 1.5 \text{ Hz}, F_c = 1.5 \text{ Hz}$	15–65	127.7

misalignment effects Prabhakar et al. [6] have presented a method based on the wavelet transforms and Patel et al. [36] have presented a method based on steady state response of the rotor system.

#### 4.5. Effect of noise on time frequency techniques for fault diagnosis

A fault diagnosis technique can be applied for industrial rotors if the vibration responses contain high SNR. But, in real cases due to the existence of several origins of noise and coupled vibrations, the vibration data recorded consists of low SNR, which is inadmissible. Thus, a fault diagnosis method should be capable of distinguishing noise from the actual response. In this section by considering the effect of noise, the detection capability of the three signal processing tools is compared. Detecting faults will become a difficult task if the signals contain low SNR. SNR of a response can be varied by

$$\text{SNR} = 10 \log \left( \frac{\sigma_s^2}{\sigma_n^2} \right) \quad (20)$$

where  $\sigma_n^2$  indicates the variance of the noise response and  $\sigma_s^2$  represents the variance of the signal. For a desired SNR, and known  $\sigma_s$ , the added noise response is  $s(t) = \sigma_n R_p$ , where  $R_p$  is a random parameter with normal distribution.

The EMD of the run-up response with an added noise of SNR (30 dB) is presented in Fig. 22. Due to the presence of the noise the IMF1 and IMF2 which contain the fault information are now incapable of processing with any technique to identify the fault accurately.

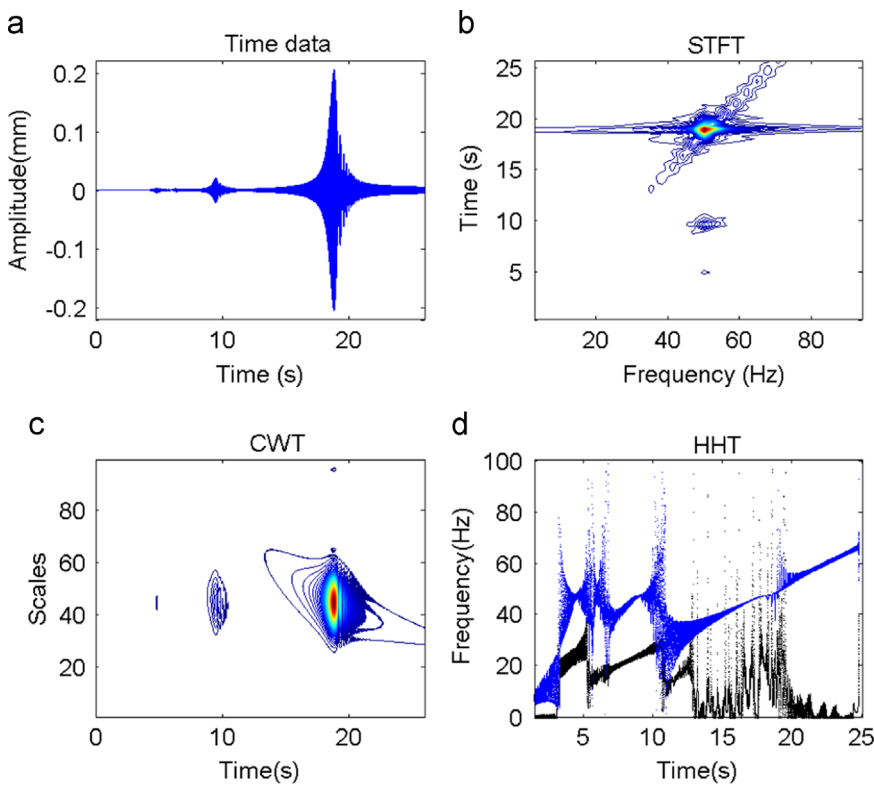


**Fig. 13.** Rotor with a large crack ( $c/D=25\%$ ).

Run-up vibration with added signal to noise ratio as shown in Fig. 21. Conventional version of HHT cannot handle low SNR. However, by denoising the signal using stationary wavelet transform one can improve the performance of the HHT. As shown in Fig. 23 for the run-up vibration signal with 30 dB added signal to noise ratio, the short time Fourier transform and Hilbert Huang Transforms could not detect the subharmonics distinctly. By using the improved Hilbert Huang Transform algorithm the fault diagnosis becomes easier even with noisy data as shown in Fig. 24. The performance of CWT based diagnosis is superior when compared to HHT approach if significant noise exists in the measured signal.

Using STFT and HHT algorithms, minimum level of misalignment detectable is presented in Table 2. CWT approach can be used to detect any level of smaller discontinuity's by zooming the scalogram as presented in previous sections. Only the resolution should be adjusted properly and requires a faster computing machine. The minimum level of crack that can be detected using STFT and HHT approaches with added SNR levels is presented in Table 3. In general, the level of noise present in the vibration response depends on the type of sensor used. Signals recorded by employing contact type sensors such as an accelerometers will yield low SNR when compared to optical sensors such as laser vibrometers or displacement proximity probes.

From the above analysis it can be concluded that due to the presence of misalignment forces the forces and moments produced in the coupling cause higher harmonics to rise at  $1/2 \times$ ,  $1/3 \times$ ,  $1/4 \times$  critical speed component of the rotor. Similar spectral characteristics are expected even if steady state vibration responses are adopted. Whereas, for different multiples of the fundamental frequencies, the frequency domain features will be distinct, the alignment solution employed for an operating frequency may not reduce the higher harmonics at other frequencies [14].

Clearly, the effect of three faults can be distinguished by employing the run-up response of the rotor. Whereas, using steady state vibration coupled with Fourier spectrum based approach for diagnosis will not reveal the presence of faults very clearly. Hilbert–Huang Transform is an empirical approach which is efficiently suitable for multiple fault diagnosis in rotor bearing systems if SNR is high.

## 5. Experimental results

### 5.1. Details of test setup

A rotor supported on two single row ball bearings with a rigid disk at the rotor center is considered for experimental investigation. The run-up vibration data obtained from the rotor bearing system are used to diagnose misalignment and rotor-stator rub faults. A picture of the experimental setup is presented in Fig. 25. The specifications and details of the

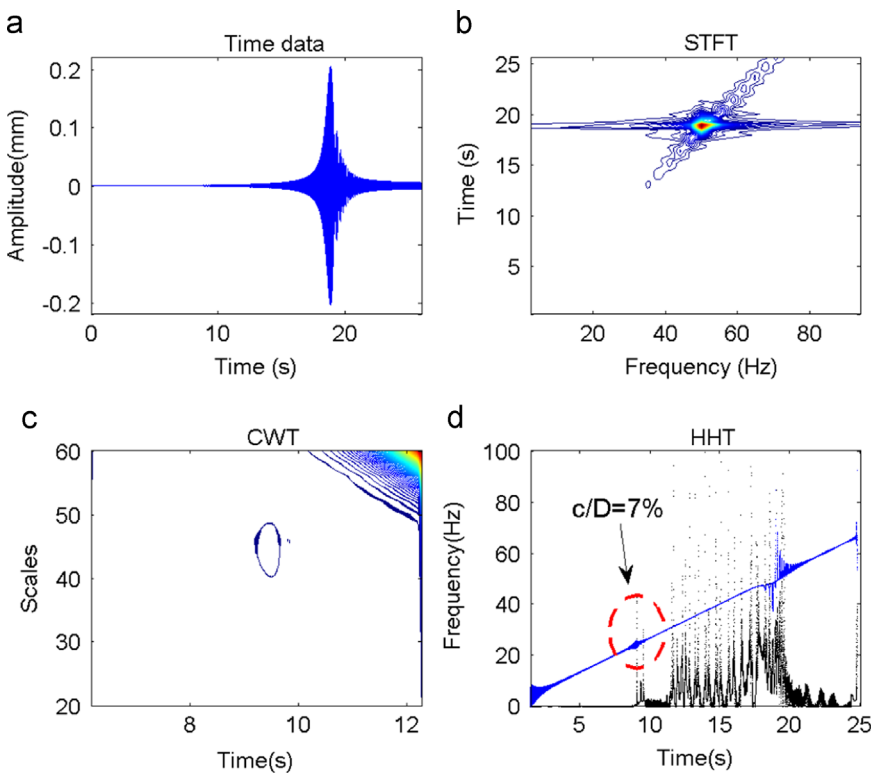


Fig. 14. Rotor with smaller crack ( $c/D=7\%$ ).

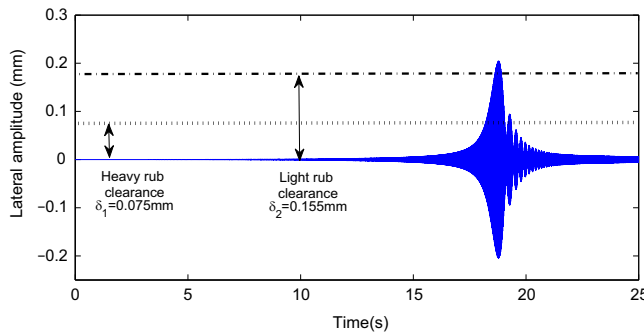
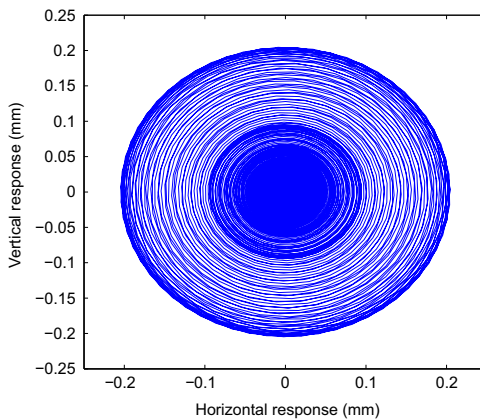


Fig. 15. Lateral run-up response and the clearance borders for heavy and light rub cases.

experimental setup are presented in Table 4. The effective length of the mild steel shaft (bearings center to center distance) is 0.72 m length and the diameter of the shaft is 0.016 m. The rotor is equipped with ball bearings (single row) at both ends. The motor drive shaft is connected to the shaft bearing assembly using spring type flexible coupling. The angular acceleration ( $\alpha$ ) of the rotor bearing system is varied using a frequency controller attached to the motor. A Polytech make optical Laser vibration measurement probe (RL 5500) is used to record the run-up vibration data of the rotor.

A rotor foundation platform connected to alignment screws is used to introduce required type and level of misalignment into the system. Both angular and parallel misalignment are introduced into the system using the alignment screws. This secondary platform is firmly attached to the primary foundation of the rotor bearing system. Alignment screws are used to introduce misalignment and after adding the required amount of misalignment, dial indicators and displacement proximity sensors are used to measure the introduced amount of misalignment. The DC voltage output from the displacement proximity sensors connected to a data acquisition system is used to record the gap voltages and these voltage readings are used to quantify the actual amount of misalignment introduced into the system.

In general, a rotor-bearing system can be subjected to annular rub or radial point rub depending upon the stator position relative to the rotor. In this paper the radial point rubbing phenomenon is considered for study. To induce rubbing, a frame as shown in Fig. 25(b) is attached to the setup. Since the rub impact is an elastic phenomenon the longitudinal stiffness ( $AE$ )



**Fig. 16.** Orbit response of the rotor without rotor–stator rub fault.

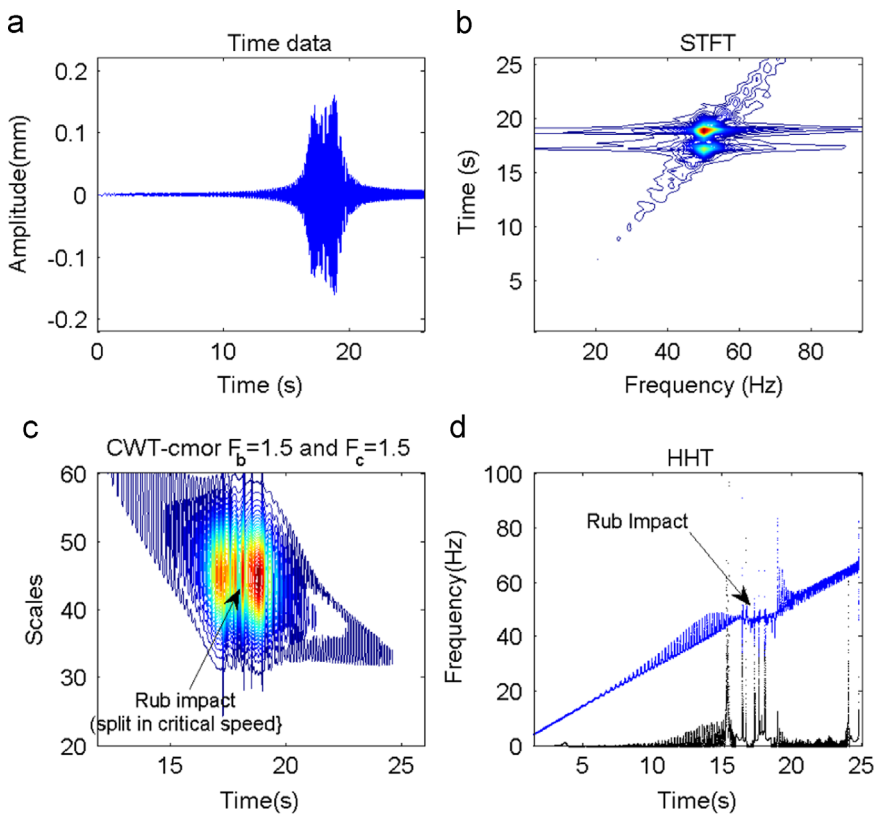


**Fig. 17.** Rotor subject with heavy rubbing forces  $\delta=0.075$  mm for  $\alpha=20$  rad/s $^2$ .

$L$ ) can be considered as the stiffness of the stator, where  $A$  is the cross sectional area,  $E$  is Young's modulus and  $L$  is the length of cylindrical stator. Two different stator materials with different lengths are considered for the study.

### 5.2. Experimental results: no fault case

The run-up data obtained for different fault cases are processed using Short Time Fourier Transform, Continuous Wavelet Transform and Hilbert Huang Transforms to study the transient harmonic behavior introduced by the faults. STFT maintains equal resolution for the full signal since the window size is constant for all frequencies. This disadvantage can be solved if wavelet transforms are used. However, wavelet transform has its own drawbacks that the wavelet coefficients depend on the proper choice of the mother wavelet function and only the response features that match with the configuration of the mother wavelet produce higher value of inner product. EMD technique does not involve the concept of basis function to capture the signal characteristics, it is a self-adaptive algorithm. As presented in Section 4, a similar approach to extract the

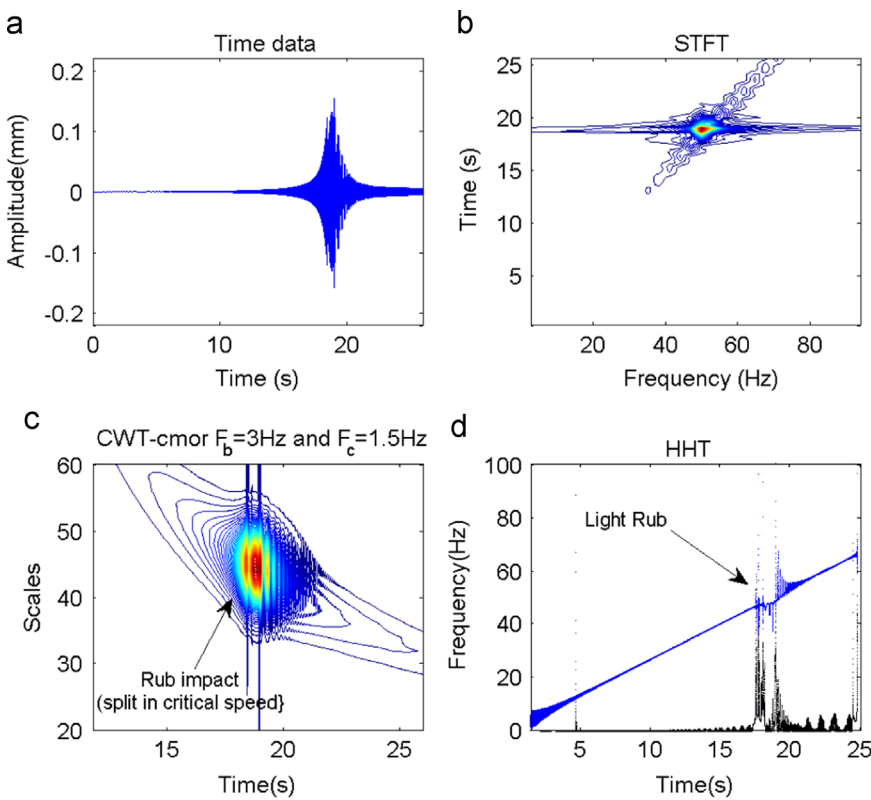


**Fig. 18.** Rotor subject with light rubbing forces  $\delta=0.155$  mm for  $\alpha=20$  rad/s<sup>2</sup>.

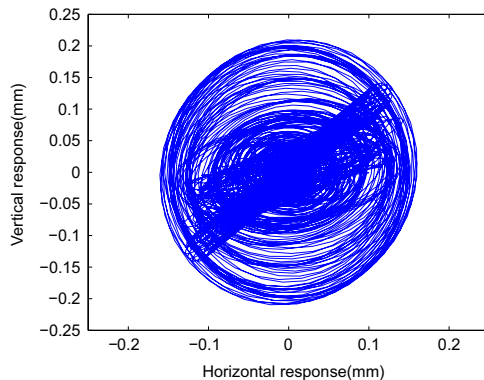


**Fig. 19.** Orbit response of the rotor with heavy rubbing forces.

Intrinsic Mode Functions of the vibration data is used to select an IMF which is capable of detecting the fault details. This IMF data is the input for the HHT technique. The performance of the empirical mode decomposition depends on independence of the intrinsic mode functions. The IMF data decomposed from EMD should not lose any energy content to avoid poor diagnosis. The run-up vibration data of the system without faults is presented in Figs. 26(a) and 27(a). This case represents the healthy state of rotor bearing system. The first four IMFs for this response are presented in Fig. 26. The corresponding STFT, CWT and HHT results are presented in Fig. 27(b-d), no sub-critical harmonic components are observed in this case and the rotor crossed critical speed at 48.6 Hz.

### 5.3. Experimental results: misalignment detection

In this study misalignment is introduced in horizontal direction of the rotor. The misalignment can also be introduced along the vertical direction by using alignment shims. Using the EMD procedure, the four fundamental IMF components for two cases misalignment fault are as shown in Figs. 28 and 29. For the case of high misalignment, it is clearly evident that the

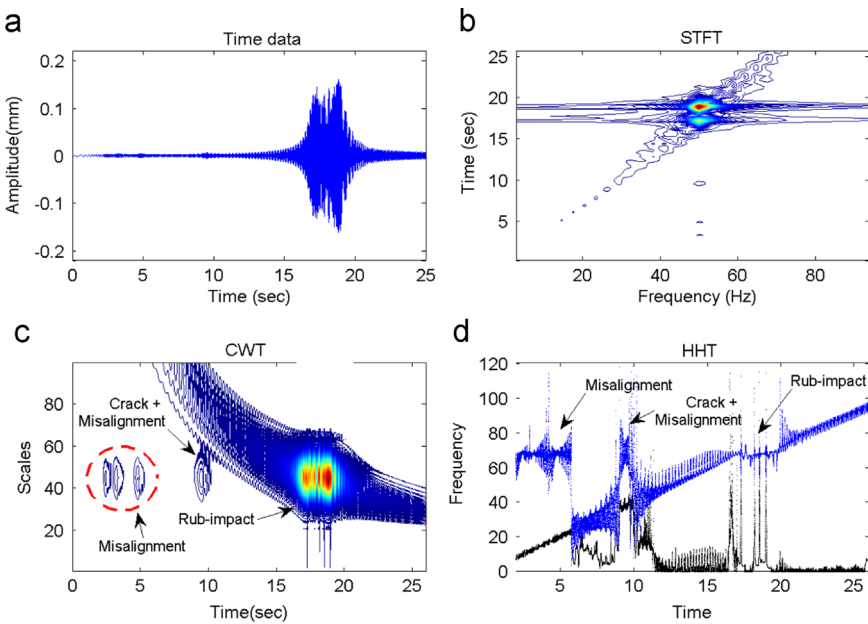


**Fig. 20.** Multiple fault diagnosis using run-up response with  $\alpha = 20 \text{ rad/s}^2$ , parallel misalignment = 0.8 mm, crack  $c = 0.12$  and rub clearance  $\delta = 0.075 \text{ mm}$ . (a) Time data, (b) STFT, (c) CWT and (d) the HHT plot-blue: IMF1 and black: IMF2. (For interpretation of the references to color in this figure caption, the reader is referred to the web version of this paper.)

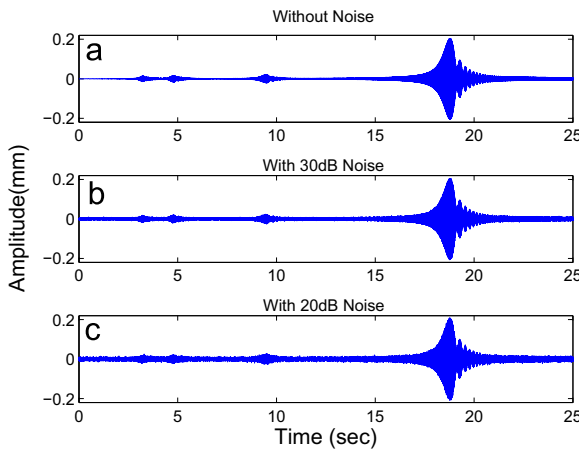


**Fig. 21.** Effect of SNR on run-up signal  $\alpha = 20 \text{ rad/s}^2$ . (a) No noise ( $\text{SNR} = \infty \text{ dB}$ ), (b) with 30 dB noise (c) with 20 dB noise (sub-harmonics masked by noise).

first IMF can clearly detect the higher harmonics developed due to the fault. Thus, IMF1 is used for HHT analysis to detect lower misalignment fault features.

The diagnosis results for the healthy rotor run-up response are as shown in Fig. 27, which also represents the results for a system without misalignment. The subharmonics are not evident for this case, however for low misalignment case (as presented in Fig. 30) and for high misalignment cases (as presented in Fig. 31) the subharmonics generated due to the fault are distinctly revealed. As per Heisenberg's time-frequency uncertainty principle, if one expects high resolution in the frequency resolution then the resolution in time domain will be poor and vice versa. The short time Fourier transform and continuous wavelet transform are based on the convolution integral and thus the concept of time-frequency resolution applies. On the other hand, the HHT technique is based on the instantaneous frequency of the responses. The estimation of instantaneous frequency is very important to detect minor changes in frequency components, which cannot be estimated using other time-frequency techniques. The HHT technique even for low level of misalignment case is powerful when compared to STFT and CWT algorithms as presented in Fig. 31.

By adjusting the resolution of the mother wavelet, CWT based approach can detect any level of existing fault. Due to the insufficient resolution parameters of the Morlet wavelet transform, the low misalignment features could not be identified as seen from Fig. 31. Improving the resolution parameters of the CMOR (Complex Morlet) function as presented in Fig. 32 the

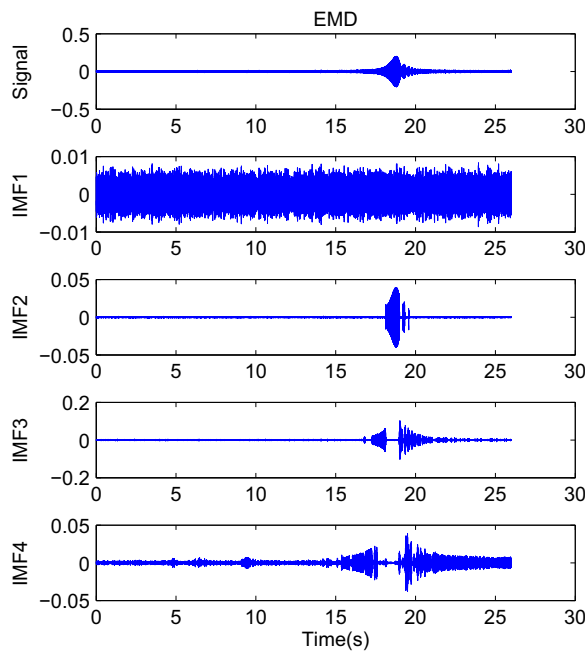


**Fig. 22.** EMD of signal with noise with 30 dB SNR.

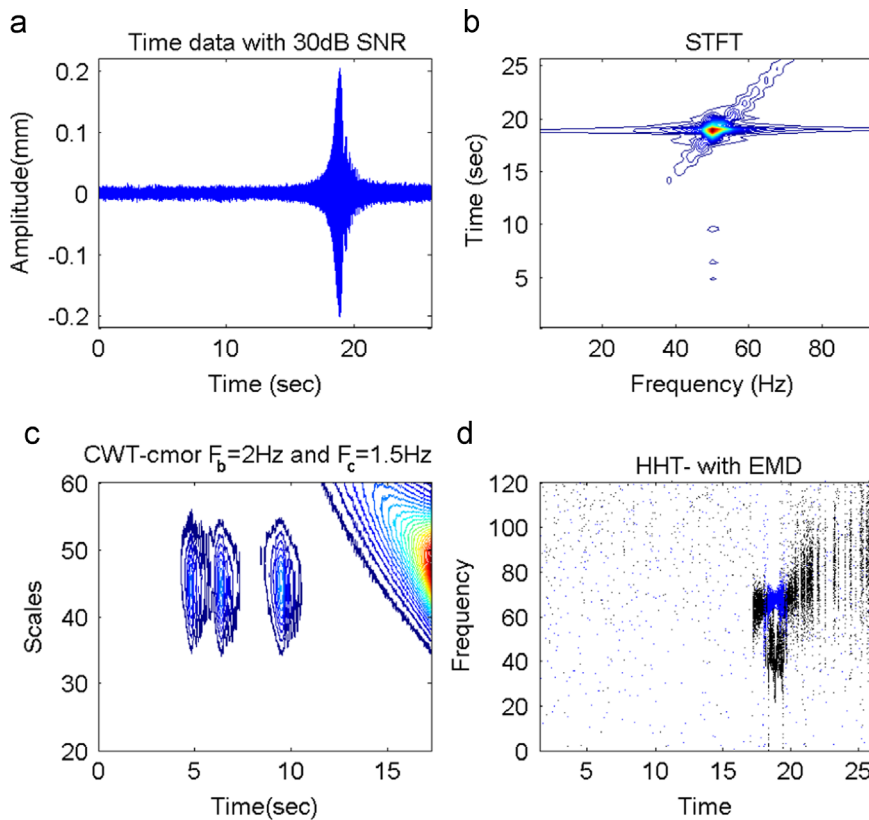


**Fig. 23.** HHT with EMD parallel misalignment results with  $\text{SNR}=30 \text{ dB}$ ,  $\Delta x=0.05 \text{ mm}$  and  $\alpha=20 \text{ rad/s}^2$ .

sub-critical harmonics are very clearly identified. Considering the improved resolution parameters the response without misalignment (see Fig. 27) has been checked for the presence of sub-critical harmonics and presented in Fig. 33. As expected the figure shows no subharmonics indicating no misalignment. The harmonic features developed for angular and parallel

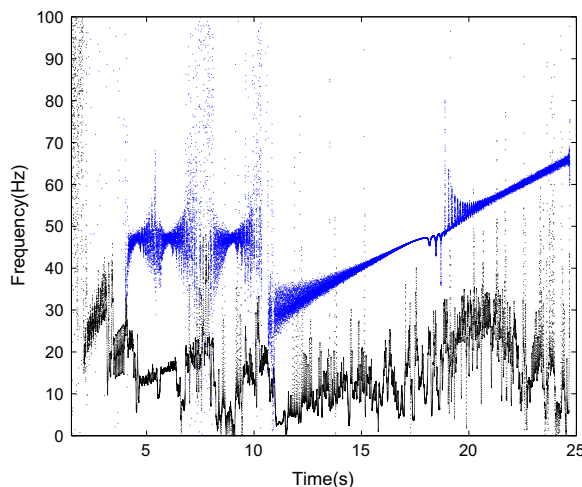


**Fig. 24.** Diagnosis results for de-noised run-up response for the HHT plot-blue: IMF1 and black: IMF2. (For interpretation of the references to color in this figure caption, the reader is referred to the web version of this paper.)

**Table 2**

Lowest amount of misalignment detectable using STFT and HHT with respect to different SNR values.

SNR (dB)	STFT (mm)	HHT (mm)
$\infty$ (no noise)	0.8	0.01
50	0.91	0.031
40	0.99	0.04
30	1.03	0.05
20 (high noise)	1.07	0.067

**Table 3**

Minimum size of crack ( $c/D \%$ ) detected for different noise levels.

SNR (dB)	STFT (%)	HHT (%)
$\infty$ (no noise)	15	7
50	17	10
35	20	12
20 (high noise)	25	14

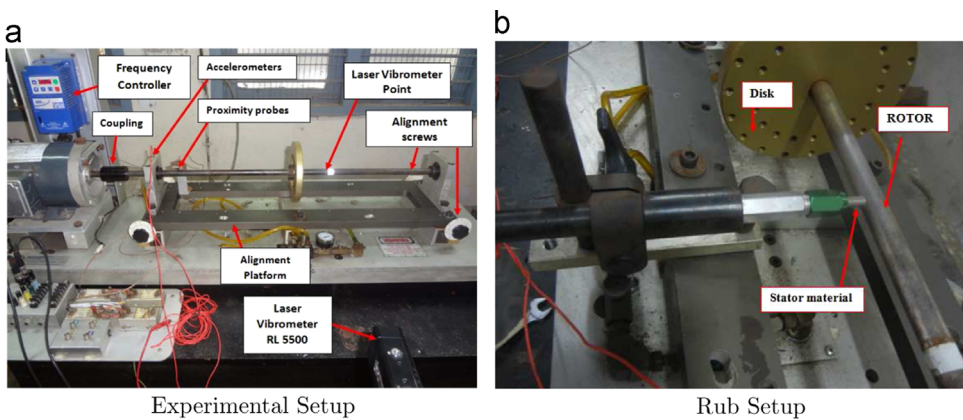


**Fig. 25.** (a) Experimental setup and (b) rub impact setup.

**Table 4**  
Physical details of the rotor bearing system.

Feature	Value (units)
<b>Rotor shaft</b>	
Length	0.72 m
Diameter	$15.810 \times 10^{-3}$ m
Density of steel	7800 kg/m <sup>3</sup>
Modulus of elasticity ( $E$ )	2,00,000 MPa
Area moment of inertia ( $I$ )	$0.3271 \times 10^{-10}$ m <sup>4</sup>
<b>Disk</b>	
Diameter	0.153 m
Mass ( $M$ )	0.892 kg
Thickness	0.016 m
Residual unbalance (me)	0.0025 kg m
Damping constant ( $C$ )	100 N s/m
<b>Motor</b>	
Speed range	0–5500 rpm
Motor power rating	0.5 HP AC, 3 Phase
Frequency controller	Delta Model VFD004S21B

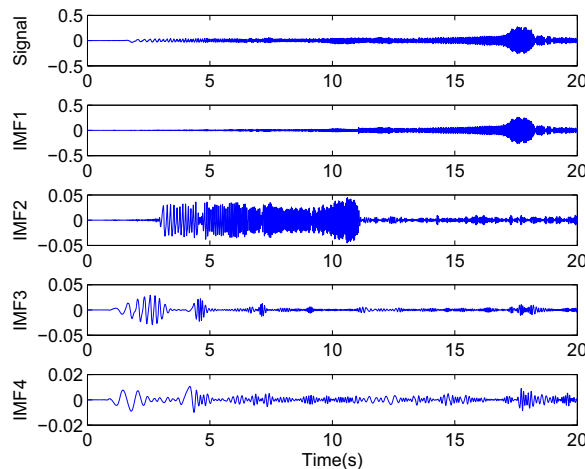


**Fig. 26.** Empirical mode decomposition of run-up response (with  $\alpha = 20$  rad/s<sup>2</sup>) for no misalignment case.

misalignment cases are distinct. However, all the three time–frequency techniques can be used for diagnosis of angular type of misalignment as presented in Figs. 34 and 35.

#### 5.4. Effect of angular acceleration on misalignment detection

The existence of subharmonics in the run-up vibration data depends on the angular acceleration of the rotor system. As presented in Fig. 36, the subharmonics indicate the level of misalignment. To reduce the misalignment present in the system the alignment task should be aimed to reduce these subharmonics. However, if  $\alpha$  is high then the existence of all the subharmonic harmonic components cannot be confirmed because the rotor will vibrate at a frequency for a very short duration of time and misalignment diagnosis cannot be pertinent. On the other hand, if  $\alpha$  is less, then the system is expected to run at frequency close to the resonance for long duration and leads to severe vibrations. For identical misalignment level (as presented in Fig. 36(b)), for different  $\alpha$  values the vibration response is presented in Fig. 36. The time–frequency diagnosis results for low and high angular acceleration cases are shown in Figs. 37 and 38 respectively. The diagnosis results for Fig. 36(b) are previously shown in Fig. 30. As shown in Fig. 38 except the HHT technique, the other time–frequency techniques could not detect the misalignment fault. Whereas, irrespective of the value of  $\alpha$  the Hilbert Huang Transform could identify the fault clearly.

#### 5.5. Rub impact detection

In this section, the experimental results for a rotor bearing system subjected to rub-impact are presented. The clearance between the stator and the rotor is measured using clearance gauges, a lower clearance between stator and rotor will yield

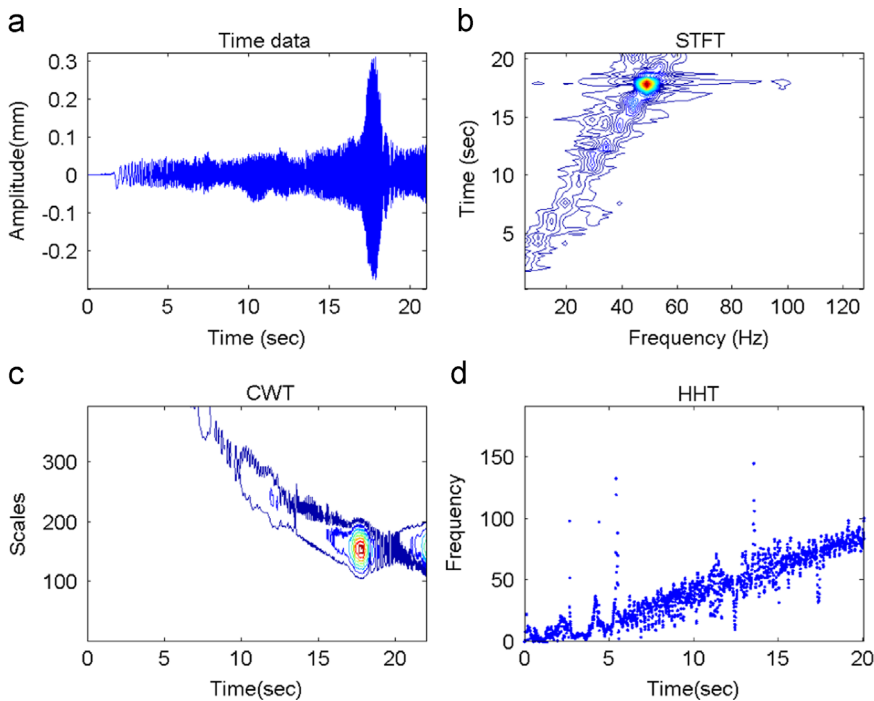


**Fig. 27.** Healthy rotor run-up response (without any fault)  $\alpha = 20 \text{ rad/s}^2$  and (a) time data, (b) STFT, (c) CWT and (d)HHT.

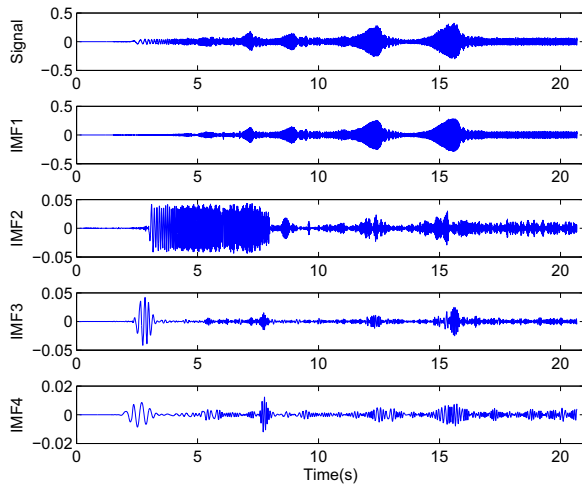


**Fig. 28.** Empirical mode decomposition of run-up response for high misalignment  $\Delta x = 1.2 \text{ mm}$  and  $\alpha = 20 \text{ rad/s}^2$ .

heavy rub and vice versa. Two levels of rub ( $\delta_1 = 0.14 \text{ mm}$  and  $\delta_2 = 0.1 \text{ mm}$ ) are considered as light and heavy rubbing cases. As discussed in Section 4.5, when significant noise is present in the response, fault detection using CWT is a preferable choice over HHT. The noise present in the signals obtained from experiments is significant. Hence, in experiments CWT is a chosen indicator for fault detection. The diagnosis results for the rub impact fault (as shown in Figs. 39 and 40) when compared to the healthy run-up response of the rotor (as shown in Fig. 27) clearly indicate the presence of rub-impact. It is observed from the results presented in Figs. 39 and 40 that rub-impact affects the response of the rotor at the resonance. An observation from experimental results a split at the critical speed is clear sign for existence of rotor stator rub impact fault. The wavelet method is observed to clearly indicate the split near resonance (see Fig. 39(c) and Fig. 40(c)). Since HHT cannot perform when noise is present in the signal CWT is always preferred.

Fan et al. [18] used the start-up vibrations for diagnosis of rotor systems equipped with journal bearings. The use of run-up responses along with new time–frequency techniques provides more information about the existing faults. Faults such as oil whirl and oil whip show different harmonic signatures which can be detected using the techniques presented in this study.

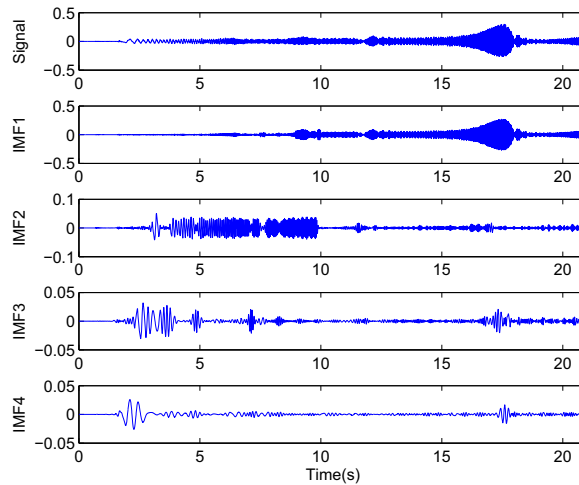


**Fig. 29.** Empirical mode decomposition of run-up response for low misalignment  $\Delta x = 0.01$  mm and  $\alpha = 20$  rad/s<sup>2</sup>.

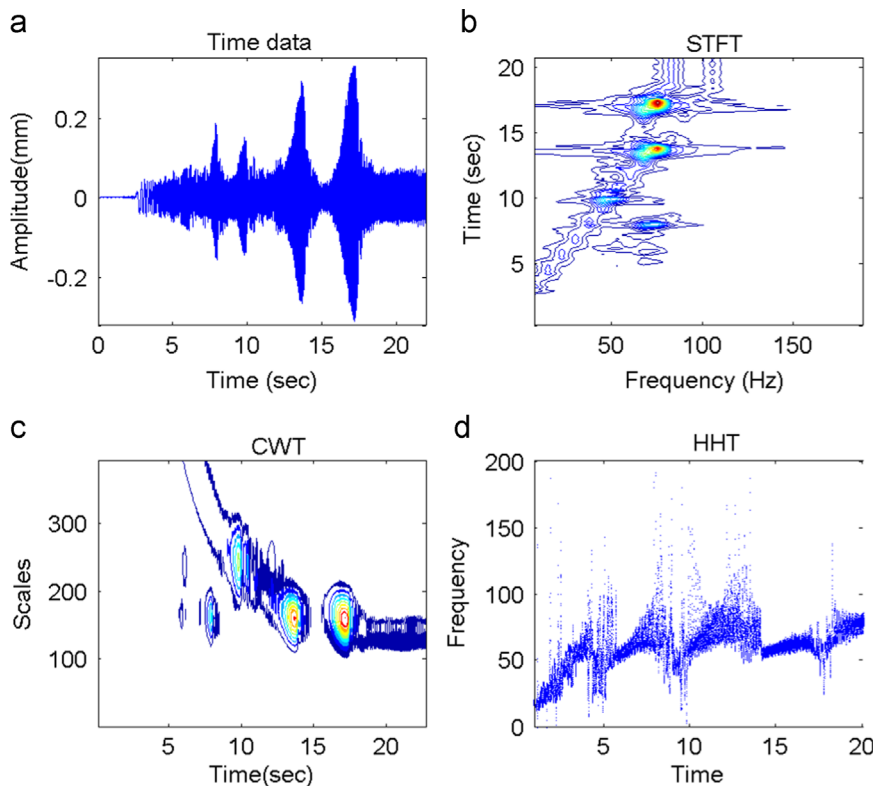


**Fig. 30.** Diagnosis results for high parallel misalignment case with  $\Delta x = 1.2$  mm, (a) run-up time data for  $\alpha = 20$  rad/s<sup>2</sup>, (b) STFT spectrogram, (c) CWT scalogram and (d) HHT for IMF1.

## 6. Conclusions

Fault diagnosing by employing run-up signals is presented in this paper. It is observed from simulation and experiments that the presence of sub-critical harmonic components indicates misalignment or a crack, while rub-impact affects the resonance region of the run-up response. Misalignment fault leads to strong sub-critical harmonics at  $0.5 \times$ , and also at other sub-harmonics. And existence of a transverse crack leads to strong sub-critical harmonic at  $0.5 \times$  and weak at other sub-harmonics of the critical speed. Three signal processing tools namely Short Time Fourier Transform, Continuous Wavelet Transform and Hilbert–Huang Transform are compared to evaluate their detection performance. The effect of Signal

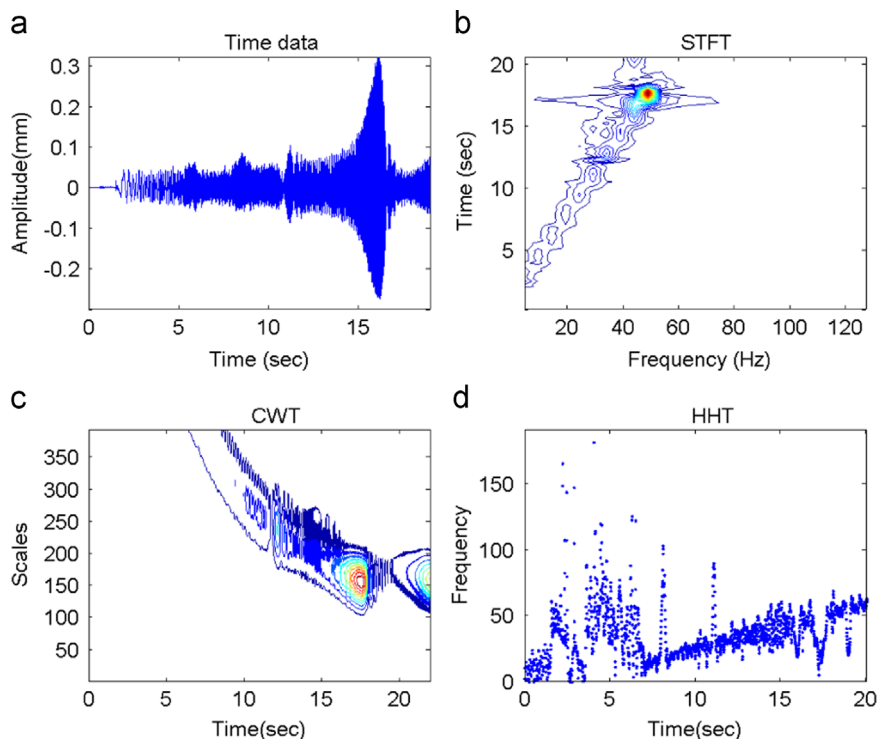


**Fig. 31.** Diagnosis results for low parallel misalignment case with  $\Delta x = 0.01$  mm, (a) run-up time data for  $\alpha = 20$  rad/s<sup>2</sup>, (b) STFT spectrogram, (c) CWT scalogram and (d) HHT for IMF.

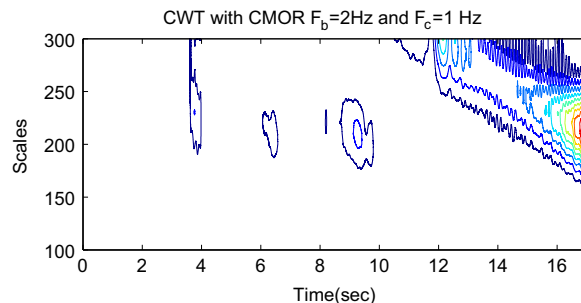


**Fig. 32.** Wavelet scalogram of truncated response (Fig. 31a) with  $F_b = 2$  Hz with misalignment fault.

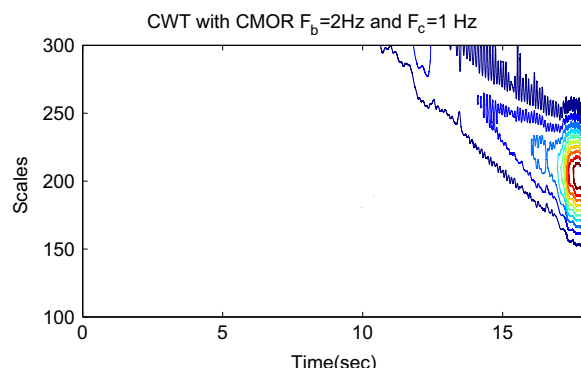


**Fig. 33.** Wavelet scalogram of truncated response of (Fig. 27a) with  $F_b = 2$  Hz for healthy rotor case.

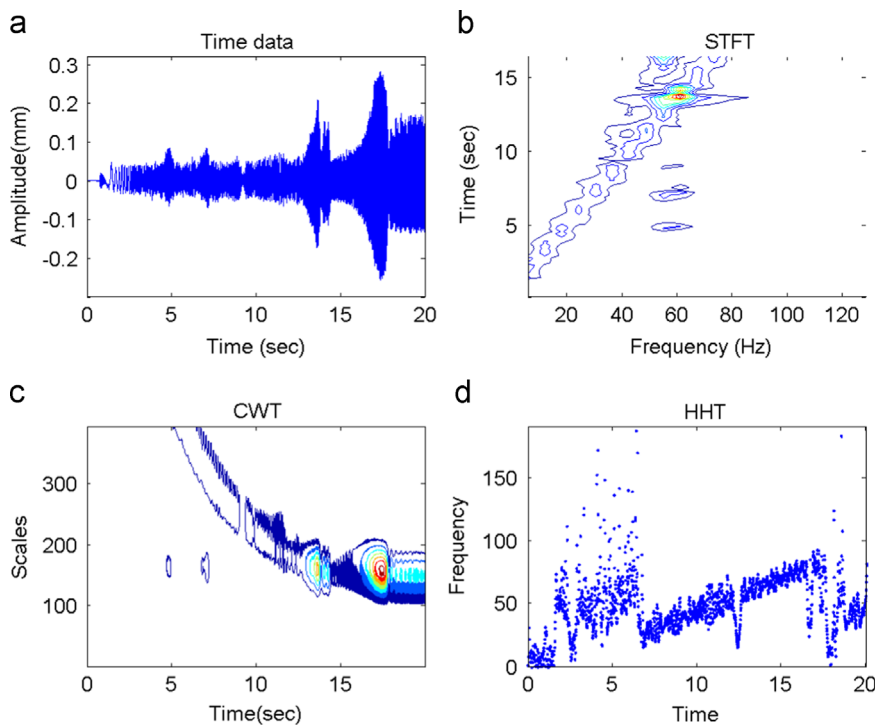


**Fig. 34.** Diagnosis results for high angular misalignment case with  $\theta = 1.5^\circ$ , (a) run-up time data for  $\alpha = 20 \text{ rad/s}^2$ , (b) STFT spectrogram, (c) CWT scalogram and (d) HHT for IMF.

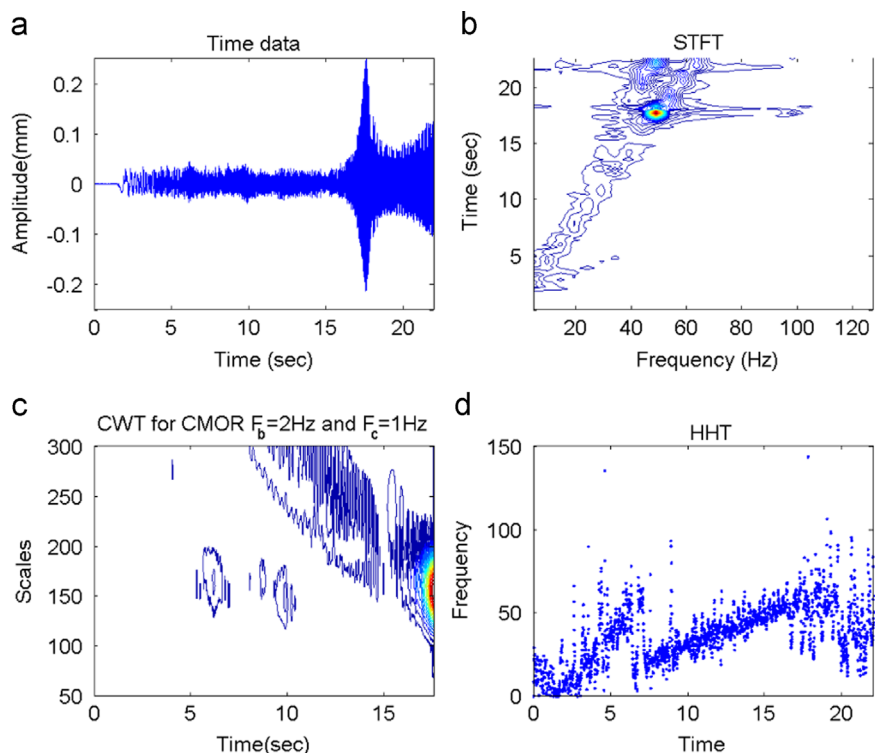


**Fig. 35.** Diagnosis results for low angular misalignment case with  $\theta = 0.5^\circ$ , (a) run-up time data for  $\alpha = 20 \text{ rad/s}^2$ , (b) STFT spectrogram, (c) CWT scalogram and (d) HHT for IMF.

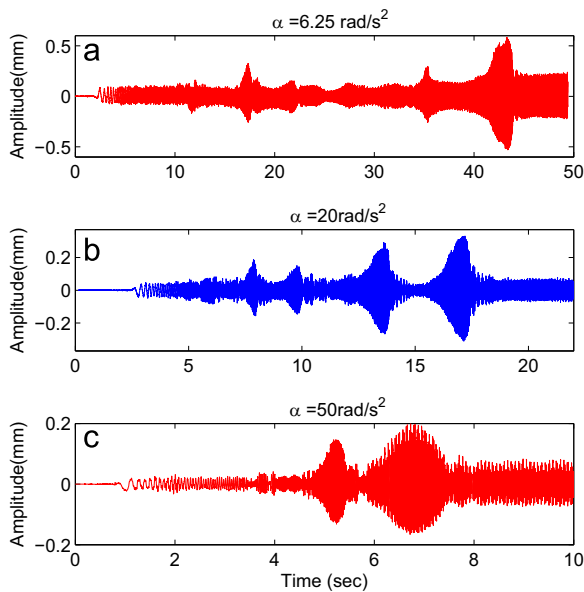


**Fig. 36.** Run-up signals for different angular acceleration for high parallel misalignment case  $\Delta x = 1.2 \text{ mm}$ , (a)  $\alpha = 6.25 \text{ rad/s}^2$ , (b)  $\alpha = 20 \text{ rad/s}^2$  and (c)  $\alpha = 50 \text{ rad/s}^2$ .

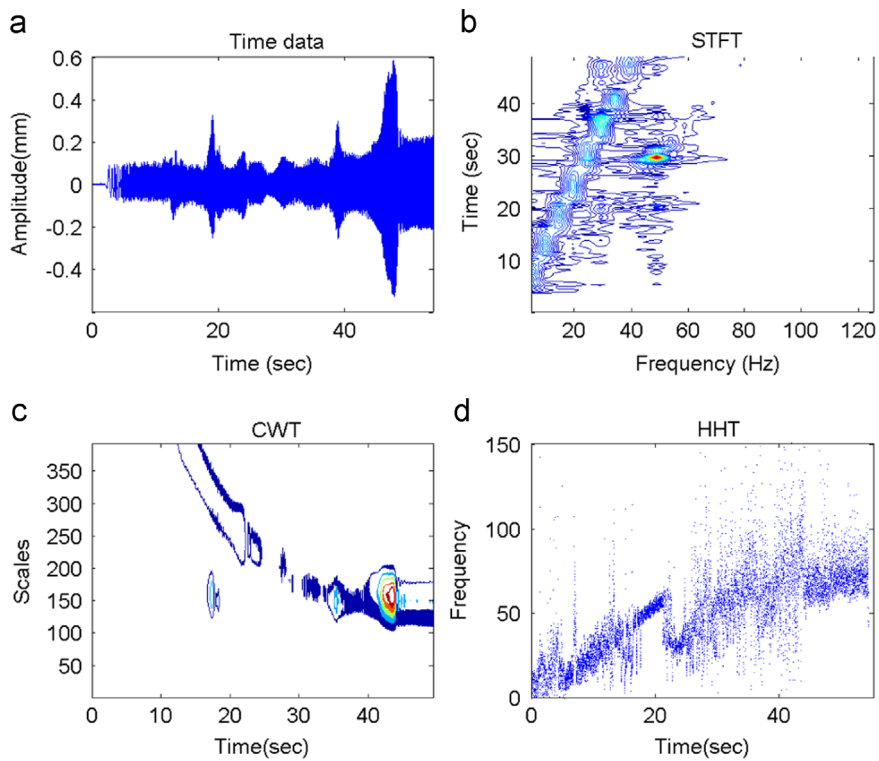


**Fig. 37.** Misalignment diagnosis for high misalignment case  $\Delta x = 1.2 \text{ mm}$  and  $\alpha = 6.25 \text{ rad/s}^2$ .

to Noise ratio and the angular acceleration on all the three techniques is presented. The comparative study of the methods is focused towards detecting the least possible level of the fault induced and the computational time consumed. When compared to CWT, HHT algorithm consumes less computation time. However, HHT algorithm is not suitable for signals with Low Signal to Noise Ratio. And while using CWT, the resolution of the mother wavelet should be adjusted properly to detect the faults. However, choosing higher values of center frequency ( $F_c$ ) and band width parameters ( $F_b$ ) the computation time

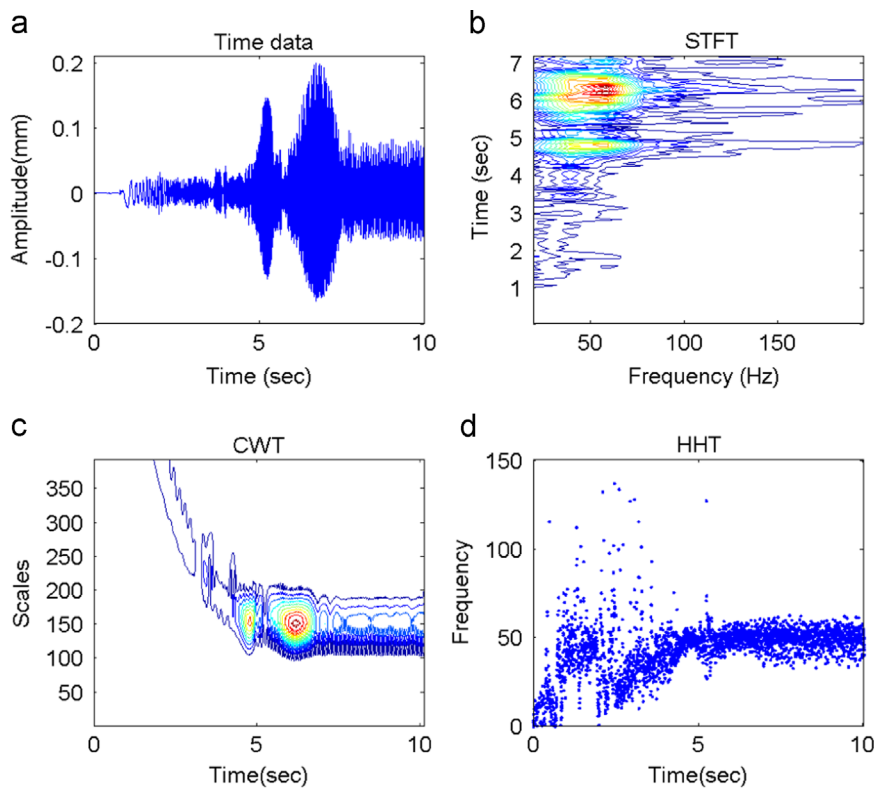


**Fig. 38.** Misalignment diagnosis for high misalignment case  $\Delta x = 1.2$  mm and  $\alpha = 50$  rad/s<sup>2</sup>.

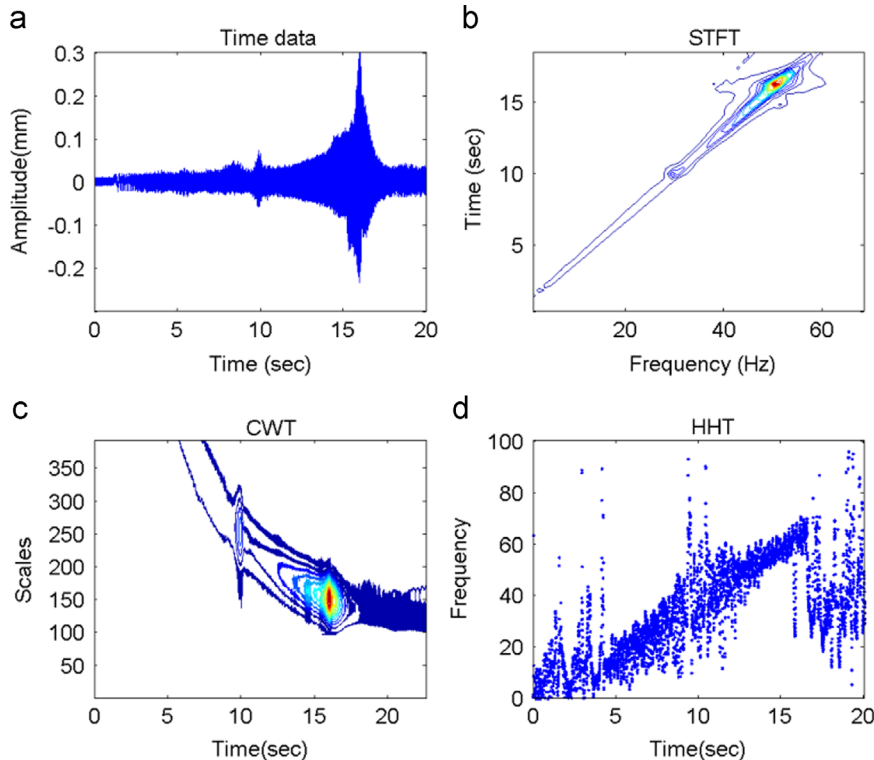


**Fig. 39.** Diagnosis results for light rub case  $\delta_1 = 0.14$  mm and  $\alpha = 20$  rad/s<sup>2</sup>.

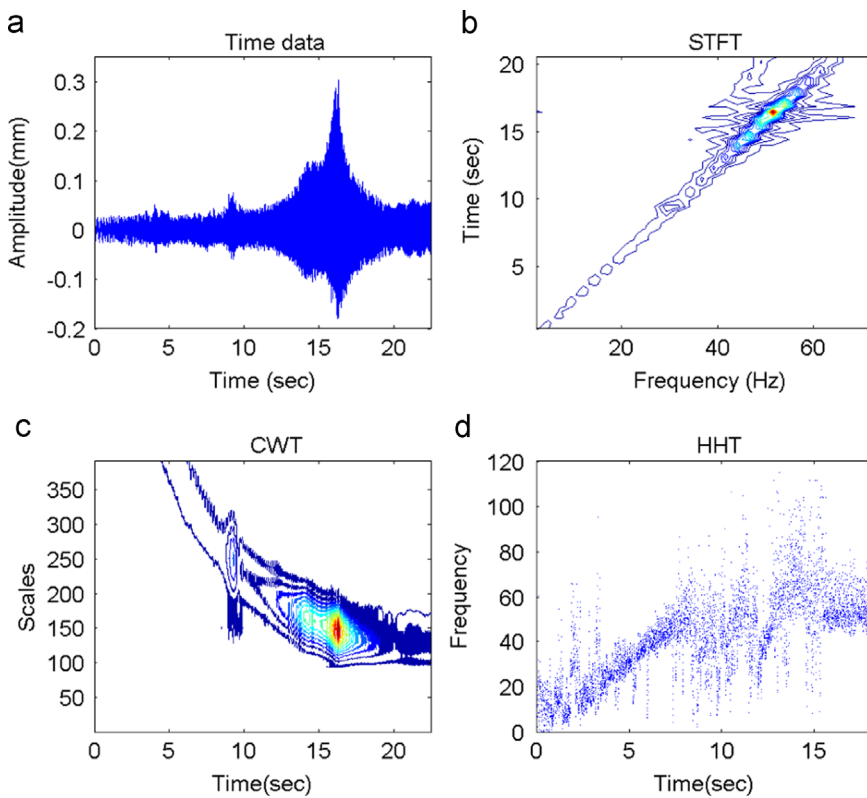


**Fig. 40.** Diagnosis results for heavy rub case  $\delta_2 = 0.1$  mm and  $\alpha = 20$  rad/s<sup>2</sup>.

increases significantly. In such cases wavelet zooming explained in this paper can be used to handle redundancy issue of the CWT and detect smaller faults.

## References

- [1] T.R. Babu, S. Srikanth, A.S. Sekhar, Hilbert Huang transform for detection and monitoring of crack in a transient rotor, *Mech. Syst. Signal Process.* 22 (4) (2008) 905–914.
- [2] T.H. Patel, A.K. Darpe, Study of coast-up vibration response for rub detection, *Mech. Mach. Theory* 44 (8) (2009) 1570–1579.
- [3] T.H. Patel, A.K. Darpe, Vibration response of misaligned rotors, *J. Sound Vib.* 325 (2009) 609–628.
- [4] B. Al-Bedoor, Transient torsional and lateral vibrations of unbalanced rotors with rotor stator rubbing, *J. Sound Vib.* 229 (3) (2000) 627–645.
- [5] J.K. Sinha, A.W. Lees, M.I. Friswell, Estimating unbalance and misalignment of a flexible rotating machine from a single run-down, *J. Sound Vib.* 272 (35) (2004) 967–989.
- [6] S. Prabhakar, A.S. Sekhar, A. Mohanty, Crack versus coupling misalignment in a transient rotor system, *J. Sound Vib.* 256 (4) (2002) 773–786.
- [7] N. Bachschmid, P. Pennacchi, A. Vania, Rotor-to-stator rub causing spiral vibrations: modelling and validation on experimental data of real rotating machine, in: Proceedings of the 8th International Conference on Vibrations in Rotating Machinery, 2004, pp. 671–680.
- [8] P. Pennacchi, N. Bachschmid, A. Vania, A model-based identification method of transverse cracks in rotating shafts suitable for industrial machines, *Mech. Syst. Signal Process.* 20 (8) (2006) 2112–2147.
- [9] P. Pennacchi, A. Vania, Diagnosis and model based identification of a coupling misalignment, *Shock Vib.* 12 (4) (2005) 293–308.
- [10] P. Pennacchi, N. Bachschmid, A. Vania, G.A. Zanetta, L. Gregori, Use of modal representation for the supporting structure in model-based fault identification of large rotating machinery: Part 1: theoretical remarks, *Mech. Syst. Signal Process.* 20 (3) (2006) 662–681.
- [11] P. Pennacchi, N. Bachschmid, A. Vania, G.A. Zanetta, L. Gregori, Use of modal representation for the supporting structure in model-based fault identification of large rotating machinery: Part 2: application to a real machine, *Mech. Syst. Signal Process.* 20 (3) (2006) 682–701.
- [12] R. Isermann, Fault diagnosis of machines via parameter estimation and knowledge processing, *Automatica* 4 (1993) 815–835.
- [13] A. Lees, J. Sinha, M. Friswell, Model-based identification of rotating machines, *Mech. Syst. Signal Process.* 23 (6) (2009) 1884–1893.
- [14] J. Piotrowski, *Shaft Alignment Handbook*, CRC Press, Florida, 2007.
- [15] J.K. Sinha, Higher order spectra for crack and misalignment identification in the shaft of a rotating machine, *Struct. Health Monit.* 6 (4) (2007) 325–334.
- [16] A.S. Sekhar, B.S. Prabhu, Effects of coupling misalignment on vibration of rotating machinery, *J. Sound Vib.* 185 (1995) 655–671.
- [17] M. Xu, R. Marangoni, Vibration analysis of a motor-flexible coupling-rotor system subjected to misalignment and unbalance: Part i: theoretical model and analysis, *J. Sound Vib.* 176 (1996) 663–679.
- [18] C.-C. Fan, Jhe-Wei Syu, Min-Chun Pan, W.-C. Tsao, Study of start-up vibration response for oil whirl, oil whip and dry whip, *Mech. Syst. Signal Process.* 25 (2011) 3102–3115.
- [19] N. Bachschmid, P. Pennacchi, A. Vania, Identification of multiple faults in rotor systems, *J. Sound Vib.* 254 (2) (2002) 327–366.
- [20] R. Yan, R.X. Gao, X. Chen, Wavelets for fault diagnosis of rotary machines: a review with applications, *Signal Process.* 96 (Part A) (2014) 1–15.
- [21] T.Y. Wu, Y.L. Chung, Misalignment diagnosis of rotating machinery through vibration analysis via the hybrid eemd and emd approach, *Smart Mater. Struct.* 18 (2009) 1–14.

- [22] G. Niu, J.-D. Son, A. Widodo, B.-S. Yang, D.-H. Hwang, D.-S. Kang, A comparison of classifier performance for fault diagnosis of induction motor using multi-type signals, *Struct. Health Monit.* 6 (3) (2007) 215–229.
- [23] C. Papadopoulos, A. Dimarogonas, Coupled longitudinal and bending vibrations of a rotating shaft with an open crack, *J. Sound Vib.* 117 (1) (1987) 81–93.
- [24] R.F. Beatty, Differentiating rotor response due to radial rubbing, *J. Vib., Acoust., Stress, Reliab.* 107 (1985) 151–160.
- [25] M. Torkhani, L. May, P. Voinis, Light, medium and heavy partial rubs during speed transients of rotating machines: numerical simulation and experimental observation, *Mech. Syst. Signal Process.* 29 (2012) 45–66.
- [26] A. Muszynska, Rotordynamics, CRC Press, Florida, 2005.
- [27] H.D. Nelson, J.M. McVaugh, The dynamics of rotor-bearings system using finite elements, *J. Eng. Ind. ASME* 98 (2) (1976) 593–600.
- [28] P. Arumugam, S. Swarnamani, B.S. Prabhu, Effects of coupling misalignment on the vibration characteristics of a two stage turbine rotor, in: ASME Design Engineering Technical Conferences, vol. 84(2), 1995, pp. 1049–1054.
- [29] C. Papadopoulos, A. Dimarogonas, Coupled longitudinal and bending vibrations of a rotating shaft with an open crack, *J. Sound Vib.* 117 (1) (1987) 81–93.
- [30] A. Sekhar, B. Prabhu, Transient analysis of a cracked rotor passing through critical speed, *J. Sound Vib.* 173 (3) (1994) 415–421.
- [31] Q. Han, Z. Zhang, B. Wen, Periodic motions of a dual-disc rotor system with rub-impact at fixed limiter, *Proc. IMechE Part C: J. Mech. Eng. Sci.* 222 (2008) 1935–1947.
- [32] Z. Feng, M. Liang, F. Chu, Recent advances in timefrequency analysis methods for machinery fault diagnosis: a review with application examples, *Mech. Syst. Signal Process.* 38 (2013) 165–205.
- [33] N.E. Huang, Z. Shen, S.R. Long, The empirical mode decomposition and the Hilbert spectrum for nonlinear and nonstationary time series analysis, *Proc. R. Soc. Lond.* 454 (1998) 903–995.
- [34] Y. Lei, J. Lin, Z. He, M.J. Zuo, A review on empirical mode decomposition in fault diagnosis of rotating machinery, *Mech. Syst. Signal Process.* 35 (12) (2013) 108–126.
- [35] D. Guo, Z. Peng, Vibration analysis of a cracked rotor using Hilbert Huang transform, *Mech. Syst. Signal Process.* 21 (8) (2007) 3030–3041.
- [36] T.H. Patel, M.J. Zuo1, A.K. Darpe, Vibration response of coupled rotor systems with crack and misalignment, *Proc. IMechE Part C: J. Mech. Eng. Sci.* 225 (2011) 700–713.